Bond Behavior of Prestressed CFRP Strips-to-Concrete Joints Using EBROG Method – Experimental and Analytical Evaluation

Niloufar Moshiri[1], Enzo Martinelli[2], Christoph Czaderski[3], Davood Mostofinejad[4], Ardalan Hosseini[5], and Masoud Motavalli[6]

Abstract

Fiber-reinforced polymer (FRP) composites are widely employed as externally bonded reinforcement (EBR) systems for strengthening of reinforced concrete members. More recently, a new technique, referred to as externally bonded reinforcement on grooves (EBROG), has been proposed, which is based on using a number of grooves throughout the concrete substrate with the aim of enhancing the bond strength between the FRP composite and concrete. This study investigates the influence of groove depth on the resulting debonding process that can be observed in prestressed carbon FRP strips. To do so, prestressing force release tests were conducted on a series of EBR and EBROG FRP strips bonded to concrete specimens. Test results demonstrated that the fracture process leading to debonding of the EBROG specimens developed in a significantly different manner with respect to the case of EBR specimens. Specifically, fractures ran through deeper layers of concrete as the grooves became deeper. Numerical analyses are also proposed to scrutinize the actual bond-slip law characterizing both EBR and

[1] PhD, Department of Civil Engineering, Isfahan University of Technology, Isfahan 15848-11888, Iran; Postdoctoral researcher, Empa, Swiss Federal Laboratories for Materials Science and Technology, Structural Engineering Research Laboratory, 8600 Dübendorf, Switzerland, niloufar.moshiri@empa.ch
[2] Department of Civil Engineering, University of Salerno, 84084 Fisciano, SA, Italy, e.martinelli@unisa.it
[3] Senior Scientist, Empa, Swiss Federal Laboratories for Materials Science and Technology, Structural Engineering Research Laboratory, 8600 Dübendorf, Switzerland, christoph.czaderski@empa.ch
[4] Professor, Department of Civil Engineering, Isfahan University of Technology, Isfahan 15848-11888, Iran, dmostofi@cc.iut.ac.ir
[5] Structural Engineer, Peoples Associates Structural Engineers, Pleasanton CA 94588, USA, ardalan.hosseini@pase.com
[6] Head of the Structural Engineering Research Laboratory, Empa, Swiss Federal Laboratories for Materials Science and Technology, 8600 Dübendorf, Switzerland, masoud.motavalli@empa.ch

This document is the accepted manuscript version of the following article:

Moshiri, N., Martinelli, E., Czaderski, C., Mostofinejad, D., Hosseini, A., & Motavalli, M. (2023). Bond behavior of prestressed CFRP strips-to-concrete joints using the EBROG method. Journal of Composites for Construction, 27(1), 2188-2196. https://doi.org/10.1061/JCCOF2.CCENG-3851

EBROG specimens. It was shown that a trilinear bond-slip law is appropriate for simulating the interface behavior in EBROG specimens.

Keywords: EBROG, prestressed FRP, bond behavior, groove depth, bond-slip analysis, bond-slip model.

Introduction

The externally bonded reinforcement (EBR) technique using fiber-reinforced polymer (FRP) systems was introduced almost three decades ago in the field of civil engineering (Meier et al. 2016). The bond behavior of FRP strips externally bonded to a concrete substrate has been investigated by various researchers, both experimentally (Chajes et al. 1996; Martinelli et al. 2011) and theoretically (Funari and Lonetti 2017; Li et al. 2022; Yuan et al. 2004) and also by considering the effect of cyclic actions (Martinelli and Caggiano 2014; Min et al. 2020). Subsequently, different test methods have been employed to study the bond behavior (Li et al. 2021; Mukhtar and Faysal 2018; Yao et al. 2005). All these studies aimed to understand the role of various parameters, possibly leading to debonding, which is often the controlling failure mode in FRP-strengthened reinforced concrete (RC) beams.

EBR FRP strips are also increasingly utilized in the form of prestressed reinforcement for the strengthening of RC beams (El-Hacha et al. 2004). In this case, the technical solution adopted for anchoring the prestressed strip to concrete and preventing the loss of bond is one of the most critical technological aspects (Grelle and Sneed 2013). Particularly, Meier and Stöcklin developed an anchoring technique referred to as "Gradient Method," which does not require any mechanical device (Meier and Stöcklin 2003). Further developments of this method were proposed by Czaderski (Czaderski 2012) and assessed by Michels et. al (Michels et al. 2014).

An alternative solution intended to enhance the bond strength of FRP systems, also in the case of prestressed strips, was first proposed by Mostofinejad and Mahmoudabadi (Mostofinejad and Mahmoudabadi 2010). It is based on using longitudinal grooves throughout the concrete surface before bonding the FRP strip so that the resulting epoxy-concrete interface is larger and more articulated. This

system is referred to as EBROG, namely, externally bonded reinforcement on grooves (Hosseini and Mostofinejad 2013).

Tajmir-Riahi et al. conducted a series of lap-shear tests to investigate the effect of the EBROG solution on the bond behavior of both FRP and steel strips bonded to concrete (Tajmir-Riahi et al. 2019). The experimental results confirmed that EBROG can outperform EBR method, particularly in the case of pre-cured FRP strips, where a significant increase in the debonding strength was observed. Another alternative to the EBR method is near-surface-mounted (NSM) reinforcement. In this method, relatively large grooves are cut in the concrete and FRP rods or narrow strips are placed inside the grooves. The NSM method is efficient in enhancing the bond strength and postponing/preventing debonding. In addition, the NSM reinforcements are well protected against vandalism because they are located inside the grooves. However, its application entails issues that make it inferior to the EBROG method. The groove dimensions are generally larger in the NSM method, and therefore require more labor, whereas in the EBROG method, grooves can be as small as 5 mm × 5 mm. In addition, cutting large grooves is not always possible because of inadequate concrete cover and the presence of steel reinforcement near the edge. Moreover, the FRP cross-sectional area that can be mounted inside the grooves in the NSM method is smaller than that of EBROG. In the EBROG method, the strip is attached on top of the grooves, and there is theoretically no limitation in the width, cross-sectional area, or the number of layers of the FRP. Furthermore, prestressing the FRP reinforcement, which is located inside the grooves, is challenging in the NSM method and requires further interventions in most cases.

Based on the results of similar lap-shear tests, Moshiri et al. performed a numerical study intended to scrutinize the bond-slip laws that can be identified for both EBR and EBROG systems (Moshiri et al. 2019). They found that the bond properties of the EBROG joints were significantly higher than those of the EBR joints, both in terms of the maximum bond strength and ultimate displacement capacity. Empirical bond strength, effective bond length, bond-slip models, and failure strain were proposed by Mostofinejad et al. for FRP sheets-to-concrete joints bonded through the EBROG method (Moghaddas and Mostofinejad 2019; Moghaddas et al. 2019; Moghaddas et al. 2021; Zamani Ghaleh and

Mostofinejad 2022). A novel suggestion by Ghahsareh and Mostofinejad addressed the classification of grooves in the EBROG method in terms of width, depth, and spacing (Mohammadi Ghahsareh and Mostofinejad 2021; Mohammadi Ghahsareh et al. 2022). They proposed longitudinal and transverse groove classes with the aim of achieving optimum collection.

Furthermore, the extension of the EBROG solution to prestressed FRP strips bonded to concrete was a natural evolution boosted by the promising results obtained for "non-prestressed" strips. Both prestressing force release tests on FRP-to-concrete joints (Moshiri et al. 2021b) and four-point bending tests on RC slabs strengthened with EBROG carbon FRP (CFRP) strips (Moshiri et al. 2020; Tehrani et al. 2019) have been carried out of comparing the performances of EBR and EBROG solutions. They clearly demonstrated that, as might have been expected, EBROG outperformed EBR in the case of prestressed FRP strips as well.

Therefore, interest has been raised in further investigating the influence of the relevant parameters on the resulting structural response of EBROG prestressed FRP strips on concrete. Specifically, attention has been focused on the role of the depth of the grooves on the resulting debonding load. Subsequently, Moshiri et al. (Moshiri et al. 2021a) executed a series of prestressing force release tests on FRP strips bonded to concrete and characterized by an invariant number of grooves of variable depths. As expected, the results of the force-slip behavior obtained from these tests were significantly affected by the groove depth.

The present paper moves from the aforementioned study by Moshiri et al. (Moshiri et al. 2021a), as an extended version of that study, and shows a detailed analysis and numerical elaborations of the prestressing force release tests initially reported therein. Specifically, it proposes the results obtained through digital image correlation (DIC) measurements, which describe pointwise the displacement fields obtained at the various stages of the prestress release procedure, up to the debonding failure of each specimen. Moreover, a numerical model already proposed in the literature (Martinelli et al. 2019) for prestressed CFRP strips bonded to steel members (Hosseini et al. 2018) was employed with the aim

of identifying the underlying bond-slip relationships for each series of prestressing release tests on specimens characterized by a given groove depth.

The current study adds new knowledge to the research on EBROG method and addresses the effect of groove depth in prestressing force release tests. More importantly, the bond behavior of prestressed FRP to concrete in the EBROG method was investigated for the first time in terms of a bond-slip model. In addition, the side-view measurement of the release test (specimen No. 11) offers instructive information on the behavior of prestressed FRP strips bonded to concrete substrate. More importantly, the bond behavior of prestressed FRP to concrete in the EBROG method was investigated for the first time in terms of a bond-slip model. It is worth mentioning that this study is a preliminary investigation on the bond behavior of prestressed FRP to concrete attached through the EBROG method. It is shown in this paper that the EBROG method significantly increases the bond strength of prestressed FRP to concrete. This indicates the potential of the EBROG method to offer a non-metallic end anchorage for prestressed FRPs, delivering advantages over the available metallic end anchors. As a result, the current study serves as the basis for further research, which is currently ongoing at the Structural Engineering Research Laboratory of the Swiss Federal Laboratories for Materials Science and Technology (Empa), Switzerland. In this new research, a novel full-composite end anchorage system is under development using the EBROG method.

Experiments

Materials

Unreinforced concrete blocks with dimensions of 1000 mm ×473 mm ×250 mm were constructed with a maximum aggregate size of 32 mm. The concrete compressive strength f'_c was determined at the time of the prestressing force release tests using three 150 mm standard cubes. Concrete blocks were strengthened with unidirectional CFRP strips 50 mm in width and 1.4 mm in thickness. According to the manufacturer, the nominal ultimate tensile strength, measured tensile elastic modulus, and fiber volume fraction were 2800 MPa, 160 GPa, and 68%, respectively (S&P Clever Reinforcement 2020). A two-

component epoxy adhesive was used in both the EBR and EBROG specimens. According to five coupon tensile tests by (Hosseini et al. 2018), the ultimate tensile strength, tensile elastic modulus, and ultimate tensile strain of epoxy adhesive were 18.9 MPa (coefficient of variation, CV = 12.4%), 9.3 GPa (CV = 3.8%), and 0.24% (CV = 20.5%), respectively.

Test procedure

To evaluate the effect of the EBROG method on the behavior of prestressed CFRP strips bonded to concrete, prestressing force release tests were performed.

The EBR and EBROG methods were used to bond the CFRP strip to the concrete. The procedures for these two methods are summarized as follows.

EBR method:

1- Surface preparation was conducted by grinding the surface and removing a thin layer.
2- The concrete surface and the CFRP strip were cleaned.
3- An approximately 2 mm thick layer of epoxy adhesive was applied on the concrete surface.
4- The CFRP strip was bonded to the top of the adhesive with a bond length of 300 mm.

EBROG method:

1- Two longitudinal grooves (along the CFRP strip direction), 10 mm in width and variable depths of 5, 10, or 20 mm, were first cut in the concrete substrate. No grinding or other types of surface preparations were performed. The groove pattern, presented in Fig. 1, consisted of two longitudinal grooves with a clear spacing of 15 mm between them and a free spacing of 7.5 mm from the strip edge.
2- The concrete surface, inside of the grooves, and CFRP strip were cleaned.
3- An epoxy adhesive was used to fill the grooves completely. an approximately two mm-thick layer of the same epoxy adhesive was immediately applied on the concrete surface.
4- Finally, the CFRP strip was bonded on top of the adhesive with a bond length of 300 mm.

It is worth noting that in all specimens the groove lengths exceeded the bond length. Therefore, the adhesive at the end of the bond area was not restrained by the concrete. This free space at the end of the bond area eliminates any possibility of restricting the shear deformation of the adhesive inside the grooves.

The prestressing force release test setup is shown in Fig. 2. The successive stages in the prestressing force release test were as follows:

1- Prestressing step. The strip was bonded to the surface and pulled by hydraulic cylinders (actuators) to a predefined prestressing force, F_p.
2- Curing step. To ensure complete curing of the adhesive, the prestressing force kept constant in the whole strip for one week at room temperature.
3- Releasing step. The prestressing force was gradually released from one side of the strip by reducing the oil pressure in hydraulic cylinder No. 2, whereas the force on the other strip end was approximately constant (see Fig. 3).

Forces in both free ends of the strip were measured using two 150 kN load cells. An example of the force changes at both strip ends during the releasing step, measured by load cells 1 and 2, is plotted in Fig. 3 for specimen EBR-2. In the prestressing step, the interfacial stresses between the FRP and concrete were zero, as the adhesive was completely uncured. Therefore, the forces in the entire FRP length and in the two load cells were similar. To keep the force constant during curing, a nut was fixed behind the steel I-column (visible in Fig. 2) so that the force was transferred from the nut to the steel column to ensure that it remained unchanged. Then, the oil pressure in the hydraulic cylinder was released during the curing period. After curing, the hydraulic cylinder was reincorporated into the setup for release. For this purpose, the oil pressure in the cylinder was again increased (resulting in a force increase of approximately 8 kN for about 230 s, as shown in Fig. 3) to loosen the nut, open it completely, and reintegrate the cylinder in the setup. Thus, the prestressing force of the right end of the FRP in Fig. 2 was held by the cylinder. Finally, the oil pressure in hydraulic cylinder 2 was gradually decreased to resemble the

release of the prestressing force. Both prestressing and releasing steps were performed in in a load-controlled mode by manually increasing/reducing the oil pressure in the hydraulic cylinder.

As shown in Fig. 3, before starting the test in the releasing step, the prestressing force was 48.8 kN. During the release of the force, the force in load cell 2 decreased, whereas the force in load cell 1 remained approximately constant. Then, at a specific load release, the CFRP strip was completely detached from the concrete substrate, indicating that the bond between the strip and the substrate that carried the load had been lost. This was considered failure of the bonded system. At this stage, the prestress force was directly transferred to load cell 1 and therefore, both load cells showed identical force levels owing to the fact that the CFRP bond to concrete substrate was completely gone. The difference between the prestressing force (F_p) and the existing force at the releasing end at this failure stage (i.e., force in load cell 2), was assumed to be the bond resistance.

3D DIC Measurements

Three-dimensional full-field deformations were measured using a 3D digital image correlation (DIC) system (ARAMIS 2008). A random high-contrast speckle pattern was applied on the surface of the specimen using a white brush, followed by an airbrush to produce black spots. A field of 350 mm ×350 mm was monitored using two digital cameras, each with a resolution of 4 megapixels. In accordance with the DIC manual, the angle between the axes of the two cameras facing the specimen surface was 25°. For the 50 mm focal lenses, the spacing between the two cameras was 580 mm, and the distance from the cameras perpendicular to the surface of the specimen was 1280 mm. Before starting the test, a calibration procedure with a special calibration panel was performed according to the manufacturer's instructions. Subsets of 15×15 pixels with a transition step of 13 pixels were generated to calculate the deformations. Capturing consecutive images from the measurement field and comparing them with the first image exactly before starting the test (i.e., unloaded image) revealed how much deformation occurred at each load level. In specimens 1 to 10, the cameras were mounted on top of the specimens, and the displacements in the top view of the specimens were measured using DIC. However, in specimen 11, in which the strip was bonded at the edge of the concrete block, the side views were monitored using

DIC. The instrumentation used in test 11 is discussed later in this paper. Using the 3D-DIC measurement system, both in-plane and out-of-plane deformations were measured to help interpret the prestress force-releasing behavior. According to the manufacturer's instructions, the displacement accuracy of the measurement system is between 0.01–0.1 pixel and 0.1–1.0 pixel for in-plane and out-of-plane deformations, respectively. Because the measurement field was 350 mm × 350 mm, which was captured by a 4 megapixels camera (2000×2000 pixels), the accuracy level was 0.002–0.018 mm and 0.018–0.175 mm for in-plane and out-of-plane deformations, respectively.

Test program

An overview of the test program, including eleven prestressing force release tests, is presented in Table 1. The specimens are labelled according to the strengthening method, that is EBR or EBROG, followed by groove dimensions (groove width × groove depth) in the EBROG method and a number showing the repetition of similar tests. For instance, "EBROG-10×5-2" refers to the second specimen among those strengthened according to the EBROG method with a groove width of 10 mm and a groove depth of 5 mm.

The CFRP strip was generally attached to the middle of the concrete substrate in specimens 1–10 (see Fig. 4). However, in specimen 11, labeled EBROG-10×10-Side, the strip was bonded along the edge of the concrete block. A unidirectional CFRP strip was bonded onto the concrete block such that the fibers were aligned in the loading direction and the shorter block edge. The test setup and results for this specimen are discussed in a separate section. It is worth mentioning that the specimens herein were partly reported in previous publications by the authors of this paper (Moshiri et al. 2021a; Moshiri et al. 2021b). However, further results and a detailed discussion are provided herein. Moreover, a numerical approach to determine the bond-slip model of prestressed FRP bonded to concrete using BEEROG method was proposed for the first time in this paper.

Experimental results and discussion

Bond resistance and failure mode

A summary of the test results is presented in Table 2, which reports the initial prestressing level of the specimens in terms of the prestressing load, prestressing ratio compared to the ultimate tensile strength of the strip, and pre-strain. It can be seen that the prestressing ratio for the EBR specimens was on average 26% (corresponding to a pre-strain of 0.0045), whereas higher prestress levels were selected for the EBROG specimens. It was mentioned that the prestressing ratio should be sufficiently high to ensure failure during release, and therefore, to represent a full prestressing force release test. Therefore, higher prestressing ratios should have been imposed on the EBROG specimens to ensure failure. Moreover, a higher release capacity was predicted by increasing the groove depth. Therefore, a 65% prestressing ratio (corresponding to a pre-strain value of 0.0114) was imposed on the EBROG specimens with 10 mm ×20 mm grooves.

The bond resistances of all the specimens are listed in Table 2 and illustrated in Fig. 5. It can be seen that the EBR specimens had resistances of 39.3, 29.6, and 48.3 kN, which are quite variable. Explanations are provided in the following where the failure modes are discussed. Conversely, EBROG specimens of the same series demonstrated similar bond resistances. Moreover, it is shown that the EBR specimens demonstrated similar load-displacement behavior as they experienced local debonding during the releasing stage and again resisted an increased load level.

The bond resistances for the EBROG specimens with 10 mm × 5 mm grooves were 55.5, 70.0, and 73.4 kN (Table 2 and Fig. 5). In addition, the EBROG specimens with 10 mm × 10 mm grooves exhibited maximum resistances of 79.7 and 83.1 kN. Increasing the groove depth to 20 mm in specimens EBROG-10×20-1 and EBROG-10×20-2 resulted in bond resistances of 110.3 and 98.5 kN, respectively. The results showed that the bond resistances of the EBROG specimens with 10 mm × 5 mm, 10 mm × 10 mm, and 10 mm × 20 mm groove dimensions were 66.3, 81.4, and 104.4 kN on average. This indicates an increase rate of 70%, 108%, and 167% compared with the average resistance of the EBR specimens.

In other words, the resistance was enhanced by factors of 1.7, 2.1, and 2.7 for the different groove dimensions, over that of the EBRs. Deepening the groove further enhances the transfer of bond stresses through a larger area in the concrete substrate, which is confined by the surrounding concrete. Therefore, the fracture energy required for the failure of the bond line tends to increase. A higher fracture energy corresponds to a higher load capacity. In addition, the cracked surfaces of the EBROG specimens, in contrast to those of the EBR specimens, were larger and deeper.

The failure modes of all the specimens are shown in Fig. 6. As shown in Fig. 6, in the EBR-1 and EBR-2 specimens, the CFRP strip was detached from the substrate in a thin layer beneath the bond area. However, debonding in the third specimen of this series, that is, specimen EBR-3, was deeper and more extensive than in the first two. This larger failure plane corresponds to a higher bond resistance in EBR-3. In the second half of the bond length in specimen EBR-3, however, cracking propagated neither very deeply nor extensively to the sides. It was deduced that the debonding mechanism of a prestressed FRP includes the formation of tensile cracks in the concrete substrate. In addition, the failure path is dependent on the aggregates position, as shown in the side view measurements section. As a result, the load transfer path, failure mode, and bond resistances could be variable. This was pronounced in EBR specimens as the debonding crack occurred in a thin layer of concrete beneath the strip.

In contrast, debonding in the EBROG method occurred in the concrete bulk beneath the grooves, indicating that the fracture depth was larger than the groove depths. The measured fracture depths were 15, 25, and 31 mm for groove depths of 5, 10, and 20 mm, respectively. As a rough estimation, it can be recognized that the fracture plane depth lies approximately 10 mm beneath the groove depth. The fracture plane in the EBROG method spread to the sides of the bond line, resulting in a very large cracked area. Fig. 6 shows that the EBROG specimens with 10 mm × 5 mm grooves experienced a larger crack width than the strip width (i.e., 50 mm) only in the second half of the bond area, starting 150 mm from the releasing end. Moreover, increasing the groove depth to 10 and 20 mm led to an even larger crack width compared with that of the 5 mm groove depth. In these cases, massive cracking was observed from the releasing end and propagated extensively to the sides and along the bond line.

As shown in Fig. 6, some of the specimens experienced wedge failure at the unloaded end. This is different from that experienced in the pulling lap-shear test, where wedge failure is probable at the loaded end and may affect the load capacity. Because the wedge failure in the prestressing force release tests was not at the loaded end, it did not affect the behavior of the specimen until the last stages before failure. In the 'crack development' section, where the propagation of cracks and failure stages are discussed, it is clear that wedge failure did not occur until the last stage (see Fig. 10).

Overall load-displacement behavior

The relative in-plane and out-of-plane deformations of the CFRP strip with respect to the concrete substrate are referred to as slip and separation, respectively. By using a 3D DIC measurement system, one can obtain 3D representations of surface strain. One longitudinal section called "Section 0" was assumed in the centerline of the CFRP strip, whereas longitudinal "sections 1 and 2" were selected on the concrete surface, away from the cracks at the last stage. Fig. 7 highlights the positions of Sections 0, 1, and 2, as well as the assumed coordinate system. The bond lengths extended ranged from x = 0 to 300 mm. The slip of the strip was simply calculated as the difference between the strip displacement in the x-direction (in Section 0) and the average of the concrete displacement in the x-direction in Sections 1 and 2. However, for out-of-plane separation displacements, the out-of-plane deformation of the strip in the z-direction was calculated and modified by considering the out-of-plane deformation and rotation of the concrete block in Sections 1 and 2 (see Fig. 7) (Czaderski 2012).

The force resistance of the CFRP-to-concrete bonded joint ΔF with respect to slip and separation of the strip at the releasing end (i.e., at x = 0 mm) is shown in Fig. 8. It can be seen from Fig. 8 that the EBR specimens experienced some plateaus before approaching their ultimate loads. Local debonding occurred during the release of the prestressing force, which could be attributed to brittle tensile cracking in the concrete. However, the behavior stabilized again and the substrate could resist higher forces after experiencing local debonding. In contrast, the EBROG specimens experienced an almost increasing trend until failure. The stiffness of the EBROG specimens decreased during the release of force. In

addition, the stiffness values of all EBROG specimens were very close to each other. The behavior of the EBROG specimens in terms of the bond-slip model is explained in the numerical modeling section.

As shown in Fig. 8 b, the separation values were much higher than the slip values for the prestressing force release tests. During force release, the eccentricity between the force (which is applied to the centroid of the FRP strip) and the concrete substrate generates out-of-plane peeling stresses in the concrete substrate, resulting in large out-of-plane deformations with respect to the substrate. It was concluded that the debonding mechanism of a prestressed FRP from concrete is not dominated by pure shear stresses, but a mixed tensile–shear mode (failure mode I/II), with the tensile mode being dominant.

Crack development

Inspecting the crack development during the releasing stage helped clarify the failure procedure in the EBR and EBROG methods. The crack development at different load levels for specimens EBR-2 and EBROG-10×10-1 are demonstrated in Fig. 9 and Fig**. 10**, respectively. The maximum principal strains, indicating cracks in the concrete, are plotted in these figures in the range of 0%–1%. The bond extended from x = 0 mm to 300 mm. As shown in Fig. 9, cracks started from the releasing end (x = 0 mm) and then propagated along the bond line as larger forces were released. Therefore, the cracked surface of the EBR-2 specimen was a rectangle beneath the CFRP strip. Although some small inclined cracks also formed, they did not propagate to the exterior sides. However, as previously mentioned, one of the three EBR specimens exhibited inclined cracking on the exterior sides (see Fig. 6c).

However, the first cracks at x = 0 mm in the EBROG specimen were inclined and tended to spread to the outer sides of the bond area (Fig. 10a). No failure occurred at this stage, and the specimen could still resist the higher released forces. Throughout the release of the higher forces, more inclined cracks were generated at the strip edges, which extended to the sides. It is clear that cracks developed beneath the strip. Finally, in the last stage, massive cracking was visible not only on the surface but also beneath the strip (Fig. 10f).

A comparison between the crack patterns of different specimens in the last stage before failure is shown in Fig. 11, indicating that all EBROG specimens failed after numerous inclined cracks appeared in the concrete. An increase in groove depth resulted in larger cracks that spread extensively to the sides. The inclined crack formation can be attributed to the stress distribution in the FRP-to-concrete bonded joints. The releasing force in the direction of the strip axis was applied to the joint with an eccentricity. The eccentricity included half of the strip thickness, the adhesive thickness, and part of the concrete depth. The eccentric load applied to the joint caused diagonal tensile stresses in the concrete substrate, resulting in tensile cracking. In the EBROG method, the adhesive thickness is larger than that of the EBR method; therefore, the stresses are transferred to deeper layers beneath the groove depth.

Side view measurements

In the context of the current research, a side view measurement was also carried out to investigate the prestress release mechanism in detail. In this test, the prestressed CFRP strip was bonded to the edge of a concrete block. By measuring the deformation on the side of the concrete block and beneath the strip, the crack formation, crack angle, crack depth and crack width corresponding to each force can be determined. The specimen and test setup for the side view DIC measurement are presented in Fig. 12. In the first step, a 20 mm-thick layer was cut from the side of the concrete block to expose the aggregates. A photograph was taken from this side view before applying black and white pattern for DIC. This photo was subsequently used to compare the development of cracks (measured by DIC) with the aggregate position beneath the bond area. In this specimen, longitudinal 10 mm × 10 mm grooves were cut near the edge (the first groove with 7.5 mm clear distance to the edge), with a similar pattern and spacing between the grooves compared with the other EBROG specimens. After filling the grooves with adhesive and bonding the strip to the surface, a prestressing force of 100.6 kN was applied to the strip. A prestressing force release test was performed after curing. The experimental results showed a bond resistance of 39.7 kN. Obviously, the debonding failure plane in this specimen was affected by the free face of the concrete block. As the FRP-to-concrete bonded joint is not confined on both sides by the surrounding concrete, the bond resistance is expected to be lower than that observed in similar EBROG

specimens. As shown in Fig. 11, the surrounding concrete is highly effective in transferring the stresses from the prestressed strip to the substrate.

The failure mode of specimen EBROG-10×10-side is displayed in Fig. 13. Deep and inclined cracking was visible in the concrete substrate. Moreover, cracks started at the beginning of the bond area and penetrated the substrate. After failure, a large concrete patch including grooves was still attached to the CFRP strip. Therefore, the failure plane formed beneath the longitudinal grooves.

The crack development in the EBROG-10×10-side specimen is shown in Fig. 14. It can be observed that one main crack was formed at the beginning of the bond length with an angle of $\alpha \cong 34°$. Overall, a crack angle of approximately $27° \leq \alpha \leq 34°$ was observed. By increasing the force ΔF, the main crack penetrated the substrate with approximately the same inclination; however, upon reaching an aggregate, its cracking path was diverted around the aggregate. This assumption was confirmed by carefully drawing the crack pattern (measured by DIC) on the photograph taken from the surface of the specimen before the test (see Fig. 14d). The crack was clearly inclined in the concrete substrate unless it faced an aggregate around which it continued at the same inclination . The groove position is shown in Fig. 14d with a green dashed line. Owing to the grooves at the beginning of the bond line, the crack was conveyed inclined to the concrete depth during the early stages. The releasing force ΔF with respect to crack width 1 at the beginning is depicted in Fig. 15. As shown in Fig. 15, the crack width is almost negligible up to $\Delta F = 20$ kN. Subsequently, the crack width significantly increased. It can be hypothesized that the cracking force in the EBROG-10×10-side specimen was approximately 20 kN.

Numerical modeling

Numerical analyses based on a simplified 1D model developed in a previous study (Martinelli et al. 2019) were proposed to further scrutinize the mechanical behavior observed experimentally. Specifically, the model is based on the following main assumptions:

1. debonding develops in pure mode II of fracture;
2. the FRP-to-concrete interface is described by a space-invariant bond-slip relationship;

3. the bond-slip relationship can be assumed by either a bi- or tri-linear expression;
4. the FRP strip behaves elastically;
5. the strip is prestressed at $\sigma_{pre} = E_f\varepsilon_{pre}$ before gluing to the concrete substrate.

Details about both its theoretical formulation and the numerical solution are omitted herein for the sake of brevity but are fully available elsewhere (Martinelli et al. 2019).

The model was employed with the aim of back-calculating the bond-slip relationships, resulting in the best fitting of the numerical simulations with respect to the related experimental results.

Fig. 16 shows the bond-slip relationships obtained from this back-calculation or "inverse identification" process. It shows that a bilinear elastic-softening law, commonly adopted for simulating the FRP-to-concrete interface behavior, can be identified for the EBR specimens. Conversely, the bond-slip relationships that lead to the best accuracy in the case of EBROG specimens are trilinear in shape, with an elastic branch followed by a constant stress plateau and a subsequent linear softening branch. Moreover, the three bond-slip laws identified for the three series of EBROG specimens are characterized by fracture energy values whose variability seems to follow the depth of the grooves.

Fig. 17 – Fig. 20 depict the comparisons between relevant experimental results and the corresponding numerical simulations. Specifically, both the release force-slip relationships ("a" graph series) and the distributions of interface slips throughout the bond length at two load levels ("b" graph series: 30 kN; "c" graph series: 55 kN, except for EBR specimens) are plotted.

The remarkable agreement between the experimental results and the numerical simulations (except for EBR-3, which exhibited a different behavior) confirms both the accuracy of the mechanical model and the consistency of the identified bond-slip laws, as shown in Fig. 16.

In addition to this empirical observation, a mechanical interpretation can be provided with the aim of further justifying the results obtained in identifying the bond-slip laws.

First, the elastic branch obtained for the EBR specimens is apparently stiffer than that identified for the EBROG specimens. This can be easily explained because in the EBROG specimens, part of the concrete

394 is replaced with epoxy, and because the epoxy is generally softer than concrete, it is reasonable to expect
395 that the slope of the elastic branch is also "softer" than the corresponding quantity obtained for EBR
396 specimens.

397 Second, the maximum bond stress tends to be higher in EBROG than in EBR, and it increases in the
398 EBROG in the case of deeper grooves. This can be justified by considering the fact (as shown in Fig. 6
399 and the bond resistance and failure mode section) that the fracture surface, which develops throughout
400 the concrete, tends to be wider in the case of deep grooves.

401 Third, the change in the shape of the bond-slip laws of EBROG with respect to the more common bilin-
402 ear law generally accepted for EBR can be interpreted on a mechanical basis. In fact, EBR specimens
403 are characterized by a smooth interface, whereas EBROG specimens have a more complex and curved
404 fracture interface. Therefore, when cracks are initiated in the EBR specimens, they encounter less re-
405 sistance to propagation. Conversely, the more complex interface of the EBROG specimens mechanically
406 behaves like a more redundant system, where stresses have a greater possibility of redistributing across
407 the interface, and crack propagation inevitably necessarily encounters more constraints.

408 Finally, it is also relevant to highlight that the four identified laws have apparently parallel softening
409 branches, and because these branches are basically controlled by the concrete toughness, it is reasonable
410 to expect a similar behavior from all the specimens, as they are made of concrete with similar strength.

411 # Conclusions

412 The present paper summarizes a detailed experimental report and proposes numerical analyses to inves-
413 tigate the mechanical behavior of prestressed CFRP strips bonded to concrete. Specifically, the response
414 of these systems subjected to prestressing force release tests was analyzed. The EBROG method with
415 different groove depth was used to bond FRP strips to concrete, and a similar case of the EBR system
416 was also considered as a reference.

417 The main conclusions can be summarized as follows:

1. The EBROG specimens exhibit a bond resistance higher than that of the EBR specimens. It is noteworthy that the EBROG method is characterized by a lower scatter in the experimental results obtained from specimens with the same groove depth.
2. The groove depth has a significant influence on the prestressing force release response of the tested specimens, as higher strengths are obtained in EBROG specimens with respect to EBR specimens, and deeper grooves also lead to higher strengths. On average, the EBROG specimens with groove depths of 5, 10, and 20 mm experienced higher bond resistances with factors of 1.7, 2.1, and 2.7, respectively, compared to the EBR specimens.
3. The experimental tests provided a detailed description of how the variation in the groove depth modifies the debonding phenomenon and, specifically, how it leads to a change in the cracking surface. The debonding crack in the EBROG specimens occurred under the grooves. Therefore, as the groove depth increased, not only a deeper but also a larger surface cracked, leading to a significant increase in resistance.
4. The side-view measurements on a specimen investigated in one of the experimental tests show in detail how the fracture response observed in EBROG specimens evolves throughout the concrete substrate, which mobilizes a very deep layer of concrete well beneath the adhesive interface. A crack angle of approximately $27° \leq \alpha \leq 34°$ was observed in the side-view measurement.
5. The numerical analyses further highlight the influence of the groove, as they lead to an apparent change in the bond-slip interaction, which is better approximated by a trilinear law than by the usual bilinear law generally accepted for EBR systems.
6. Moreover, a mechanical justification can be determined for the effects of the groove depth in terms of the reduction in the modulus of the elastic branch and the increase in both the maximum bond stress and fracture energy. The analytical back-calculation of the experimental results revealed higher bond shear stresses and higher fracture energies for the EBROG method with deeper grooves.

Finally, the present study contributes to understanding of the role of grooves in debonding failure of the EBROG system. Because the presence of grooves significantly increases the spatial development of the fracture process throughout the concrete, further studies are needed to investigate the effect of other relevant geometric parameters (e.g., the width of the CFRP strip) on the resulting behavior of EBROG systems.

Data Availability Statement

Some or all data, models, or code generated or used during the study are available from the corresponding author by request. (All the experimental data and findings of the numerical study appear in the published article).

Acknowledgments

The authors sincerely thank the technical team at the Structural Engineering Research Laboratory of the Empa, Switzerland. Financial support for performing the experiments and providing the materials by S&P Clever Reinforcement Company AG, Switzerland, is gratefully acknowledged. The first author was financed by mobility grants received from Iran's Ministry of Science, Research and Technology (MSRT), Iran's National Elites Foundation, Empa Structural Engineering Research Laboratory, and ZHAW (Swiss Leading House for research collaboration with partner institutions) for the visiting research period at Empa.

References

ARAMIS 2008. *User Manual Software v. 6.3. GOM GmbH Braunschweig, Germany, 2008*.

Chajes, M. J., Finch, W. W., Januszka, T. F., and Thomson, T. A. 1996. "Bond and force transfer of composite material plates bonded to concrete." *ACI structural journal*, 93(2), 208-217.

Czaderski, C. 2012. "Strengthening of reinforced concrete members by prestressed externally bonded reinforcement with gradient method." Ph.D. Thesis, ETH Zürich, Zürich, Switzerland, https://doi.org/10.3929/ethz-a-007569614.

El-Hacha, R., Wight, R. G., and Green, M. F. 2004. "Prestressed carbon fiber reinforced polymer sheets for strengthening concrete beams at room and low temperatures." *Journal of Composites for Construction*, 8(1), 3-13. https://doi.org/10.1061/(ASCE)1090-0268(2004)8:1(3).

Funari, M. F., and Lonetti, P. 2017. "Initiation and evolution of debonding phenomena in layered structures." *Theoretical and Applied Fracture Mechanics*, 92, 133-145.

Grelle, S. V., and Sneed, L. H. 2013. "Review of anchorage systems for externally bonded FRP laminates." *International Journal of Concrete Structures and Materials*, 7(1), 17-33. https://doi.org/10.1007/s40069-013-0029-0.

Hosseini, A., and Mostofinejad, D. 2013. "Experimental investigation into bond behavior of CFRP sheets attached to concrete using EBR and EBROG techniques." *Composites Part B: Engineering*, 51, 130-139. https://doi.org/10.1016/j.compositesb.2013.03.003.

Hosseini, A., Ghafoori, E., Wellauer, M., Marzaleh, A. S., and Motavalli, M. 2018. "Short-term bond behavior and debonding capacity of prestressed CFRP composites to steel substrate." *Engineering Structures*, 176, 935-947. https://doi.org/10.1016/j.engstruct.2018.09.025.

Li, W., Huang, P., Chen, Z., Zheng, X., Yang, Y., and Guo, X. 2021. "Bond behavior of fully bonded CFRP-concrete interface with improved double shear tests." *Journal of Building Engineering*, 43, 102866.

Li, W., Huang, P., Chen, Z., Cui, H., Guo, X., and Wu, B. 2022. "Bond–slip model considering the interface shear stress reversal phenomenon and data dispersion for FRP–concrete interface." *Engineering Fracture Mechanics*, 108492.

Martinelli, E., Czaderski, C., and Motavalli, M. 2011. "Modeling in-plane and out-of-plane displacement fields in pull-off tests on FRP strips." *Engineering Structures*, 33(12), 3715-3725. https://doi.org/10.1016/j.engstruct.2011.08.008.

Martinelli, E., and Caggiano, A. 2014. "A unified theoretical model for the monotonic and cyclic response of FRP strips glued to concrete." *Polymers*, 6(2), 370-381. https://doi.org/10.3390/polym6020370.

Martinelli, E., Hosseini, A., Ghafoori, E., and Motavalli, M. 2019. "Behavior of prestressed CFRP plates bonded to steel substrate: Numerical modeling and experimental validation." *Composite Structures*, 207, 974-984. https://doi.org/10.1016/j.compstruct.2018.09.023.

Meier, U., and Stöcklin, I. 2003. "Bonding of carbon fibre reinforced plastic (CFRP) strips on concrete with stress gradients and process control." *Proc., 21st International symposium on bonding technology: joining techniques in the building construction industry*, 47-51.

Meier, U., Brönnimann, R., Anderegg, P., Terrasi, G. P., Motavalli, M., and Czaderski, C. 2016. "Carbon fiber reinforced composites proved to be very successful in construction during a quarter of a century." *Proc., European Conference on Composite Materials, Munich, Germany; 26-30 June 2016*, 1-8. European Conference on Composite Materials, ECCM.

Michels, J., Martinelli, E., Czaderski, C., and Motavalli, M. 2014. "Prestressed CFRP strips with gradient anchorage for structural concrete retrofitting: experiments and numerical modeling." *Polymers*, 6(1), 114-131. https://doi.org/10.3390/polym6010114.

Min, X., Zhang, J., Wang, C., Song, S., and Yang, D. 2020. "Experimental investigation of fatigue debonding growth in FRP–concrete interface." *Materials*, 13(6), 1459.

Moghaddas, A., and Mostofinejad, D. 2019. "Empirical FRP-Concrete Bond Strength Model for Externally Bonded Reinforcement on Grooves." *Journal of Composites for Construction*, 23(2), 04018080. https://doi.org/10.1061/(ASCE)CC.1943-5614.0000924.

Moghaddas, A., Mostofinejad, D., and Ilia, E. 2019. "Empirical FRP-concrete effective bond length model for externally bonded reinforcement on the grooves." *Composites Part B: Engineering*. https://doi.org/10.1016/j.compositesb.2019.05.068.

Moghaddas, A., Mostofinejad, D., Saljoughian, A., and Ilia, E. 2021. "An empirical FRP-concrete bond-slip model for externally-bonded reinforcement on grooves." *Construction and Building Materials*, 281, 122575. https://doi.org/10.1016/j.conbuildmat.2021.122575.

Mohammadi Ghahsareh, F., and Mostofinejad, D. 2021. "Groove classification in EBROG FRP-to-concrete joints." *Construction and Building Materials*, 275, 122169. https://doi.org/10.1016/j.conbuildmat.2020.122169.

Mohammadi Ghahsareh, F., Mostofinejad, D., and Batebi, S. 2022. "Effects of different groove classes used in externally bonded reinforcement on grooves joints on carbon fiber-reinforced polymer-to-concrete bond behavior." *ACI Structural Journal*, 119(4). https://doi.org/http://dx.doi.org/10.14359/51734656.

524 Moshiri, N., Tajmir-Riahi, A., Mostofinejad, D., Czaderski, C., and Motavalli, M. 2019. "Experimental
525 and analytical study on CFRP strips-to-concrete bonded joints using EBROG method." *Composites Part*
526 *B: Engineering*, 158, 437-447. https://doi.org/10.1016/j.compositesb.2018.09.046.
527 Moshiri, N., Czaderski, C., Mostofinejad, D., Hosseini, A., Sanginabadi, K., Breveglieri, M., and
528 Motavalli, M. 2020. "Flexural strengthening of RC slabs with nonprestressed and prestressed CFRP
529 strips using EBROG method." *Composites Part B: Engineering*, 108359.
530 https://doi.org/10.1016/j.compositesb.2020.108359.
531 Moshiri, N., Czaderski, C., Mostofinejad, D., Hosseini, A., and Motavalli, M. 2021a. "Effect of Groove
532 Depth on Behavior of Prestressed CFRP Strips Bonded to Concrete by Using EBROG Method." *Proc.,*
533 *10th international conference on fibre-reinforced polymer (FRP) composites in civil engineering (CICE*
534 *2020/2021)*, 2188-2196. Springer, Cham. https://doi.org/10.1007/978-3-030-88166-5_189.
535 Moshiri, N., Czaderski, C., Mostofinejad, D., and Motavalli, M. 2021b. "Bond resistance of prestressed
536 CFRP strips attached to concrete by using EBR and EBROG strengthening methods." *Construction and*
537 *Building Materials*, 121209. https://doi.org/10.1016/j.conbuildmat.2020.121209.
538 Mostofinejad, D., and Mahmoudabadi, E. 2010. "Grooving as alternative method of surface preparation
539 to postpone debonding of FRP laminates in concrete beams." *Journal of Composites for Construction*,
540 14(6), 804-811. https://doi.org/10.1061/(ASCE)CC.1943-5614.0000117.
541 Mukhtar, F. M., and Faysal, R. M. 2018. "A review of test methods for studying the FRP-concrete
542 interfacial bond behavior." *Construction and Building Materials*, 169, 877-887.
543 S&P Clever Reinforcement 2020. "Technical data sheet, S&P CFRP-laminates, carbon fiber plates for
544 structural reinforcement."
545 Tajmir-Riahi, A., Moshiri, N., Czaderski, C., and Mostofinejad, D. 2019. "Effect of the EBROG method
546 on strip-to-concrete bond behavior." *Construction and Building Materials*, 220, 701-711.
547 https://doi.org/10.1016/j.conbuildmat.2019.06.065.
548 Tehrani, B. N., Mostofinejad, D., and Hosseini, S. M. 2019. "Experimental and analytical study on
549 flexural strengthening of RC beams via prestressed EBROG CFRP plates." *Engineering Structures*, 197,
550 109395. https://doi.org/10.1016/j.engstruct.2019.109395.
551 Yao, J., Teng, J., and Chen, J. F. 2005. "Experimental study on FRP-to-concrete bonded joints."
552 *Composites Part B: Engineering*, 36(2), 99-113.
553 Yuan, H., Teng, J., Seracino, R., Wu, Z., and Yao, J. 2004. "Full-range behavior of FRP-to-concrete
554 bonded joints." *Engineering Structures*, 26(5), 553-565.
555 https://doi.org/10.1016/j.engstruct.2003.11.006.
556 Zamani Ghaleh, R., and Mostofinejad, D. 2022. "Empirical expression for failure strain in EBROG-
557 bonded FRP–concrete joints." *Journal of Composites for Construction*, 26.
558 https://doi.org/10.1061/(ASCE)CC.1943-5614.0001226.

559

560

561

562 # Tables

563 **Table 1.** Test layout.

No.	Specimen label	Strengthening method	Number of longitudinal grooves	Groove dimensions		f'_c (MPa)	DIC measure-ments
				Width, b_g (mm)	Depth, d_g (mm)		
1	EBR -1	EBR	-	-	-	41.8	Top view
2	EBR-2					41.8	Top view
3	EBR-2					43.2	Top view
4	EBROG-10×5-1	EBROG	2	10	5	38.8	Top view
5	EBROG-10×5-2					41.2	Top view
6	EBROG-10×5-3					41.2	Top view
7	EBROG-10×10-1	EBROG	2	10	10	41.8	Top view
8	EBROG-10×10-2					41.8	Top view
9	EBROG-10×20-1	EBROG	2	10	20	41.2	Top view
10	EBROG-10×20-2					41.2	Top view
11	EBROG-10×10-Side	EBROG	2	10	10	43.2	Side view

564

565

566

567

568

569

570

571

572

573 **Table 2.** Test results.

Specimen label	Initial prestressing level			Bond resistance (kN)	Average bond resistance (kN)	Increase in bond resistance (%)
	Prestressing force (kN)	Ratio* (%)	Pre-strain, ε_{pre}			
EBR-1	51.9	26%	0.0046	39.3		
EBR-2	48.8	25%	0.0044	29.6	39.1	–
EBR-3	50.2	26%	0.0045	48.3		
EBROG-10×5-1	99.5	51%	0.0089	55.5		
EBROG-10×5-2	100.3	51%	0.0090	70.0	66.3	70%
EBROG-10×5-3	99.4	51%	0.0089	73.4		
EBROG-10×10-1	100.0	51%	0.0089	79.7		
					81.4	108%
EBROG-10×10-2	101.9	52%	0.0091	83.1		
EBROG-10×20-1	127.3	65%	0.0114	110.3		
					104.4	167%
EBROG-10×20-2	127.9	65%	0.0114	98.5		
EBROG-10×10-Side	100.6	51%	0.0090	39.7	–	–

574 * Compared to ultimate tensile strength, 196 kN

575

576

577

578

579

580

Figures

Fig. 1. Groove pattern in EBROG method (all dimensions are in mm).

Fig. 2. Prestressing force release test setup.

Fig. 3. Changes of the forces at both strip ends during the releasing step up to failure of the specimen (specimen EBR-2).

Fig. 4. Position of the strip on the block. (a) Specimens 1 to 10. (b) Specimen 11.

Fig. 5. Bond resistance (kN) for different groove depths in prestressing force release tests (groove depth of 0 mm corresponds to EBR specimens).

Fig. 6. Failure mode of prestressing force release tests (direction of releasing the prestressing force is illustrated in the photographs). (a) EBR-1. (b) EBR-2. (c) EBR-3. (d) EBROG-10×5-1. (e) EBROG-10×5-2. (f) EBROG-10×5-3. (g) EBROG-10×10-1. (h) EBROG-10×10-2. (i) EBROG-10×20-1. (j) EBROG-10×20-2.

Fig. 7. Coordinate system in the prestressing force release test (dimensions are in mm).

Fig. 8. Force-displacement behavior. (a) Force-slip. (b) Force-separation.

Fig. 9. Crack development during prestress force releasing for specimen EBR-2. (a) ΔF=22.0 kN. (b) ΔF=24.6 kN. (c) ΔF=27.7 kN. (d) ΔF=29.6 kN (last stage).

Fig. 10. Crack development during prestress force releasing for specimen EBROG-10×10-1. (a) ΔF=35.4 kN. (b) ΔF=47.8 kN. (c) ΔF=57.7 kN. (d) ΔF=79.7 kN. (e) ΔF=78.4 kN. (f) ΔF=79.2 kN (last stage).

Fig. 11. Crack patterns at the last stage before failure. (a) EBR-1. (b) EBR-2. (c) EBR-3. (d) EBROG-10×5-1. (e) EBROG-10×5-2. (f) EBROG-10×5-3. (g) EBROG-10×10-1. (h) EBROG-10×10-2. (i) EBROG-10×20-1. (j) EBROG-10×20-2.

603 **Fig. 12.** Test setup for the side view measurement, specimen EBROG-10×10-Side. (a) Grooves cut near
604 the block edge. (b) Position of DIC cameras.

605 **Fig. 13.** Failure mode of specimen EBROG-10×10-side. (a) Side view. (b) Top view.

606 **Fig. 14.** Crack development during prestress force for specimen EBROG-10×10-side. (a) ΔF=24.1 kN.
607 (b) ΔF=34.1 kN. (c) ΔF=39.7 kN (last stage). (d) Cracks pattern with respect to the aggregate position,
608 drawn on a photo from the concrete surface.

609 **Fig. 15.** Force-crack width of specimen EBROG-10×10-side.

610 **Fig. 16.** Bond-slip relationships identified for the four series of release tests**.**

611 **Fig. 17.** Experimental vs. numerical comparisons: EBR specimens. (a) Force-slip relationship. (b) In-
612 terface slip distribution (ΔF= 30 kN).

613 **Fig. 18.** Experimental vs. numerical comparisons: EBROG-10×5 specimens. (a) Force-slip relationship.
614 (b) Interface slip distribution (ΔF= 30 kN). (c) Interface slip distribution (ΔF= 55 kN).

615 **Fig. 19.** Experimental vs. numerical comparisons: EBROG-10×10 specimens. (a) Force-slip relation-
616 ship. (b) Interface slip distribution (ΔF= 30 kN). (c) Interface slip distribution (ΔF= 55 kN).

617 **Fig. 20.** Experimental vs. numerical comparisons: EBROG-10×20 specimens. (a) Force-slip relation-
618 ship. (b) Interface slip distribution (ΔF= 30 kN). (c) Interface slip distribution (ΔF= 55 kN).

619

620

Figure1

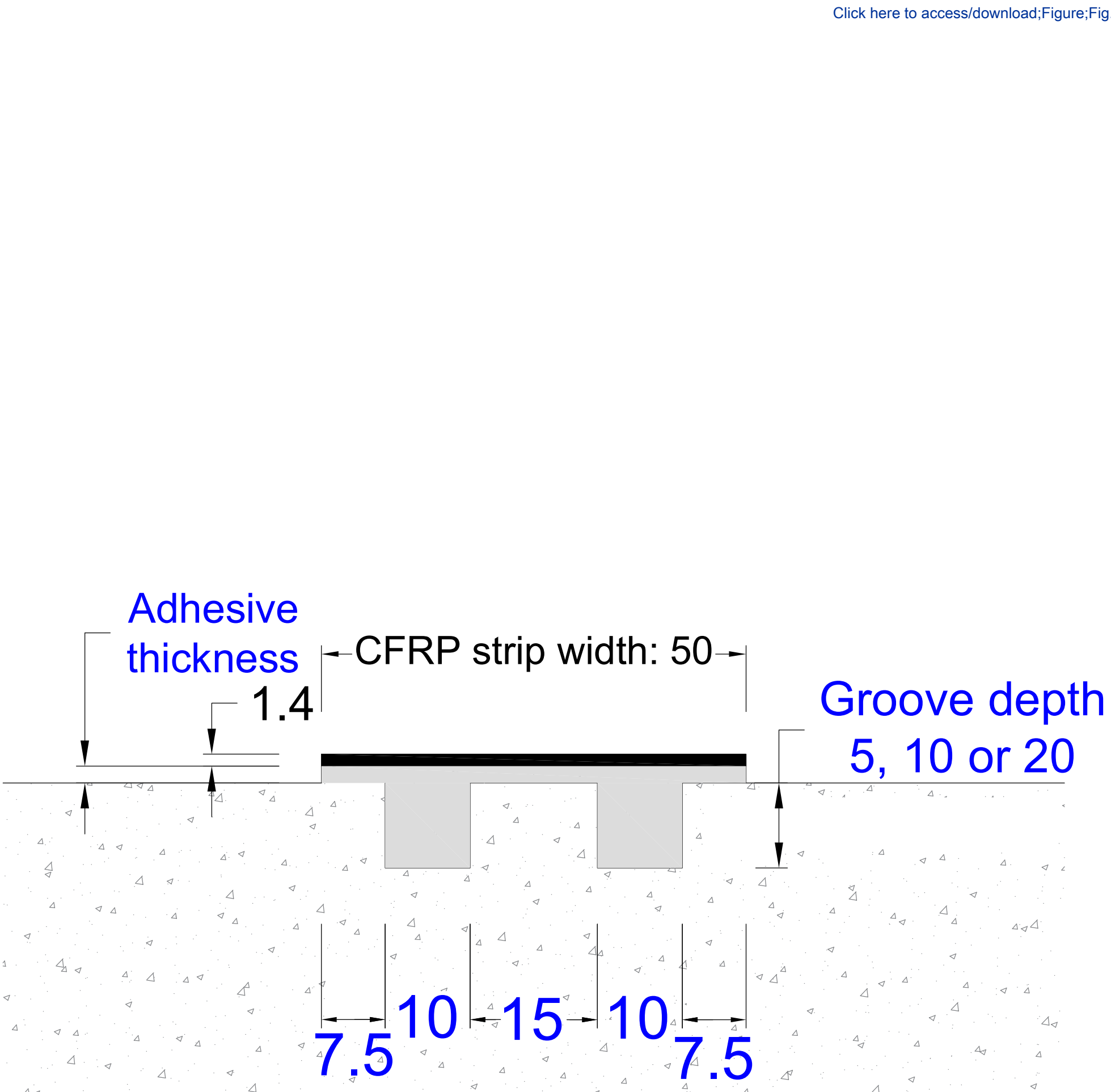

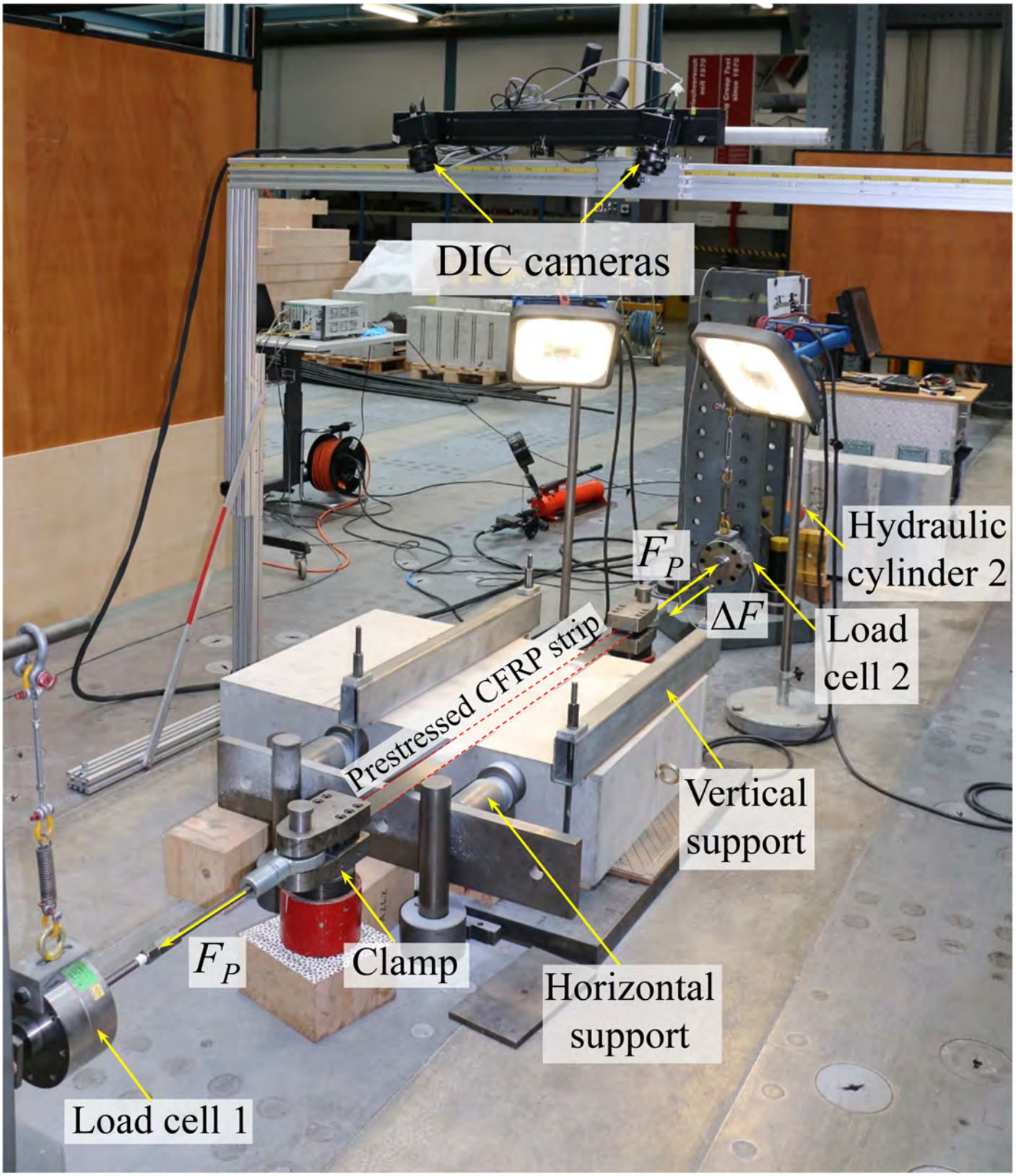

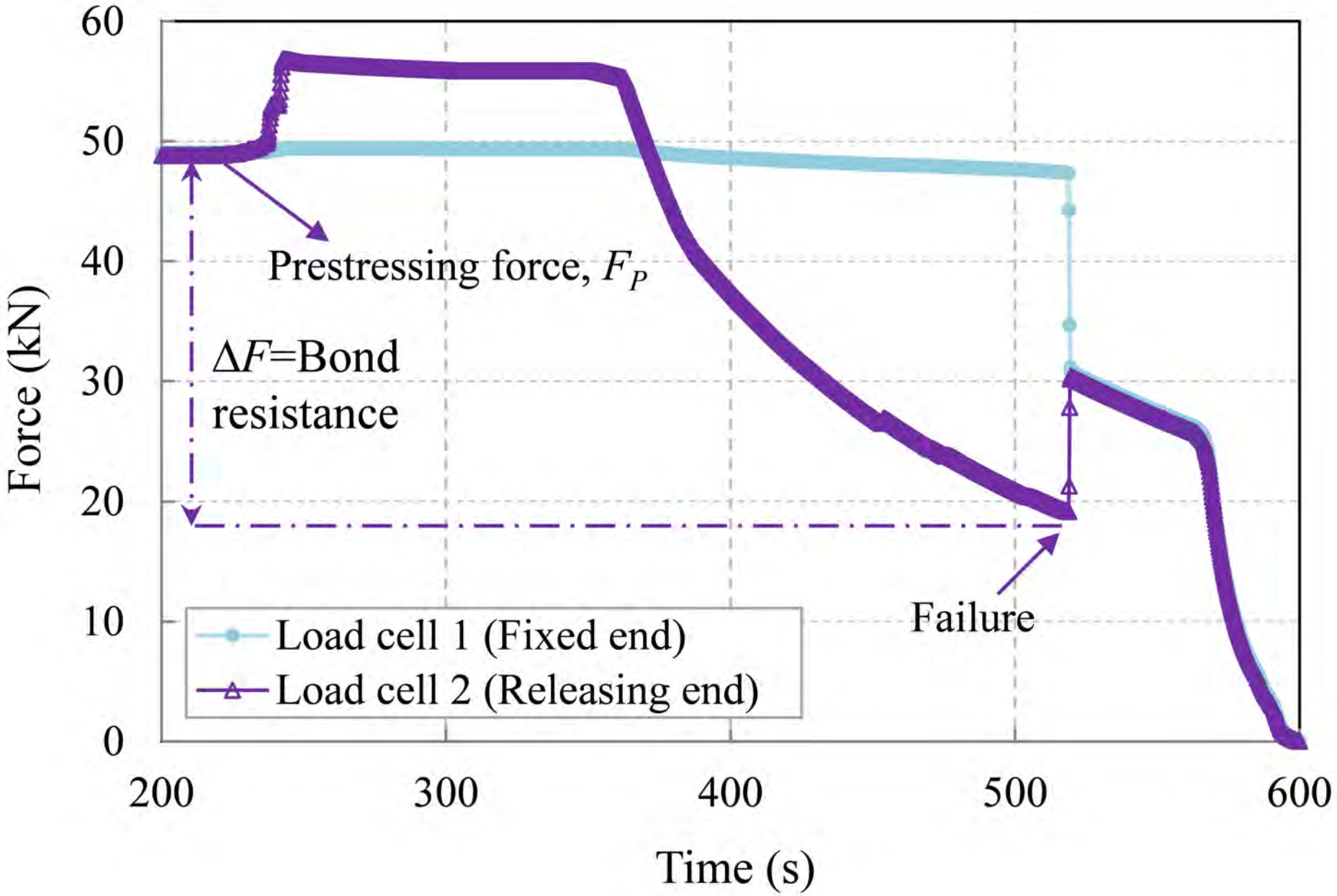

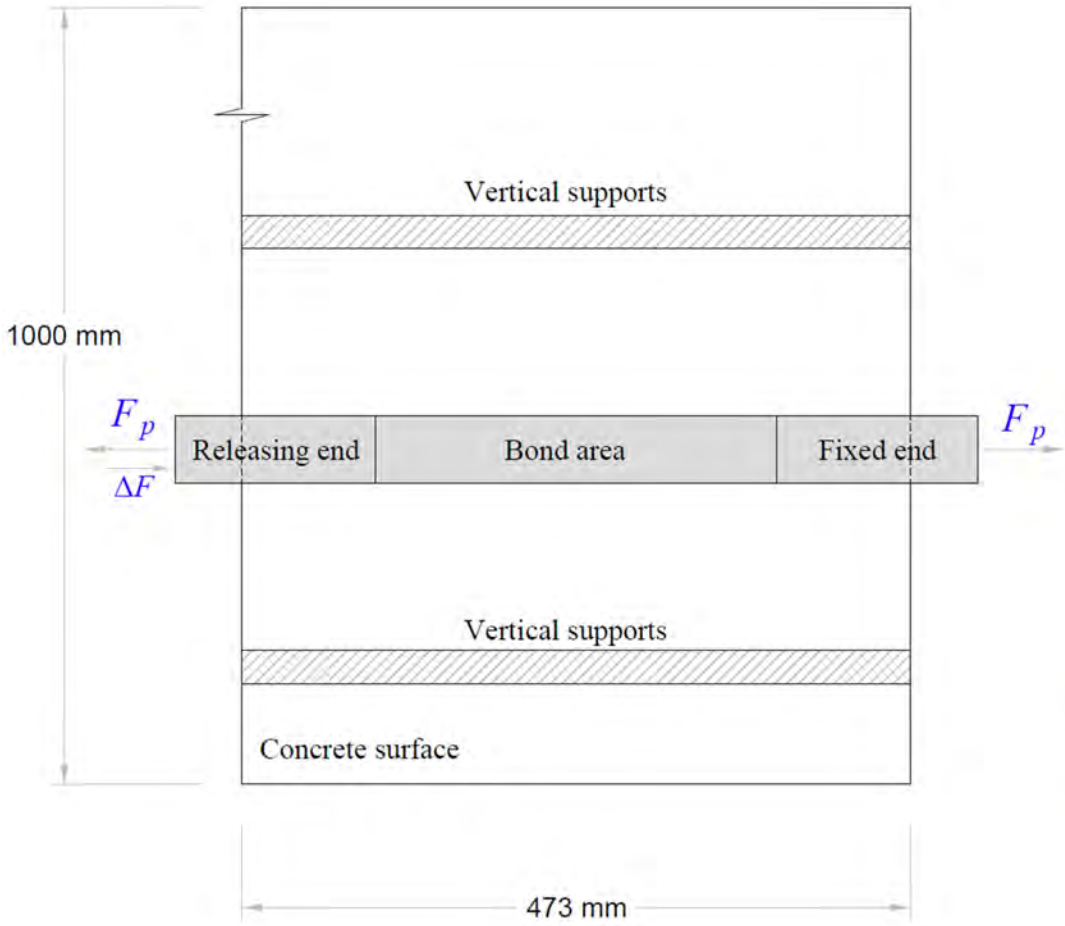

(a) Specimens 1 to 10

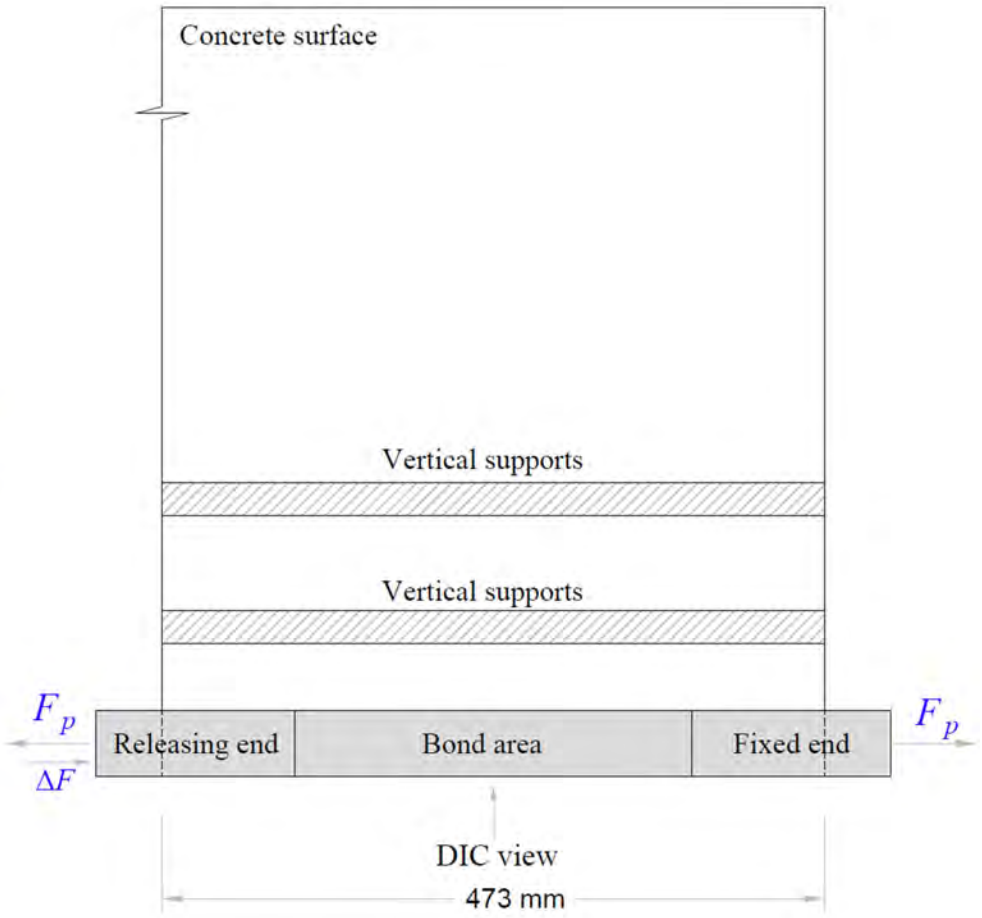

(b) Specimen 11

Figure5

Click here to access/download;Figure;Fig. 5 .pdf

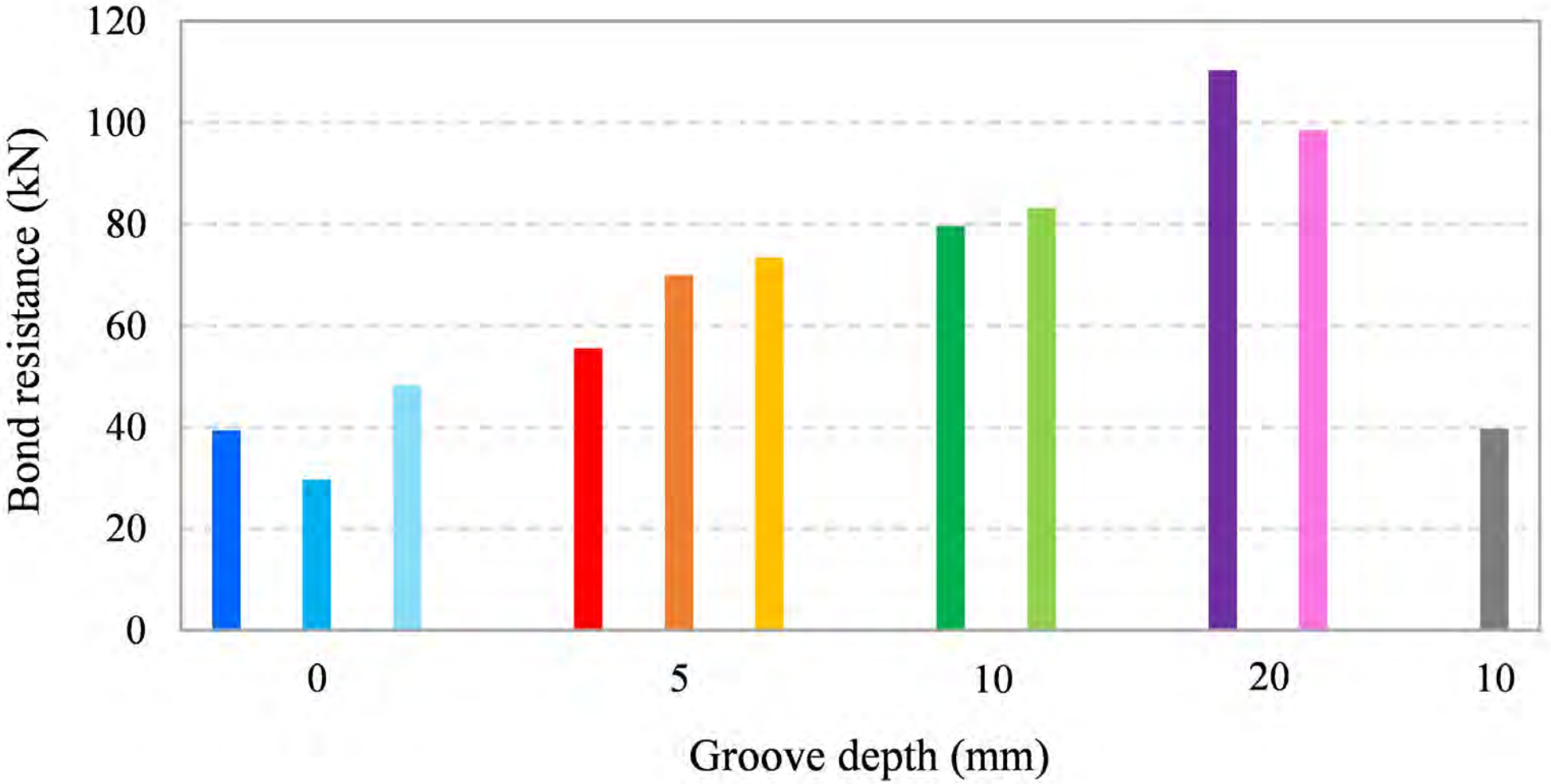

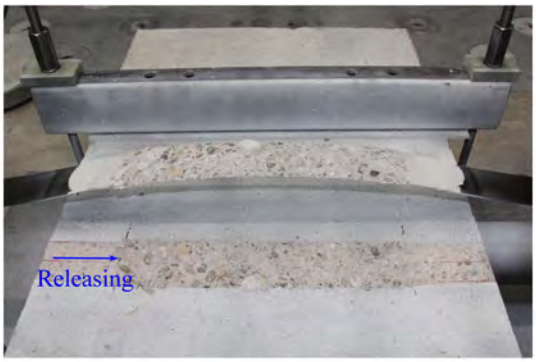

(a) EBR-1

(b) EBR-2

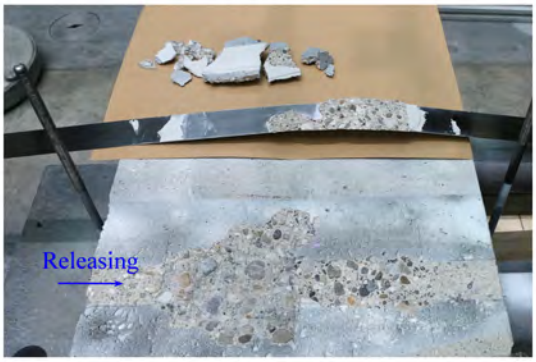

(c) EBR-3

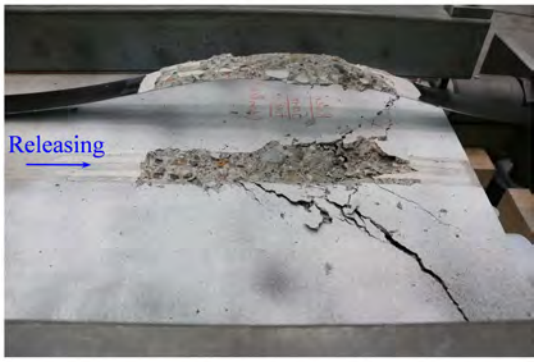

(d) EBROG-10×5-1

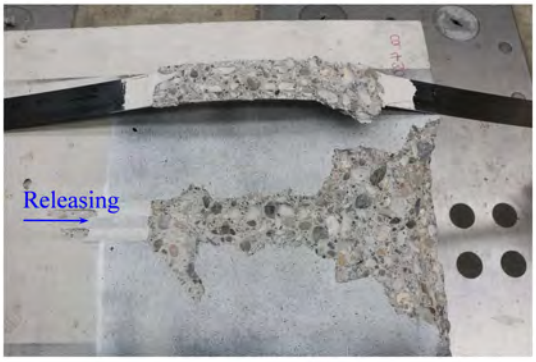

(e) EBROG-10×5-2

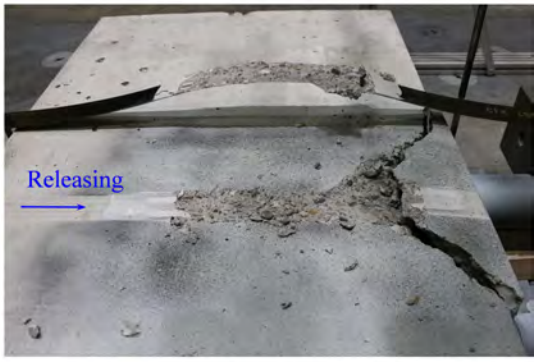

(f) EBROG-10×5-3

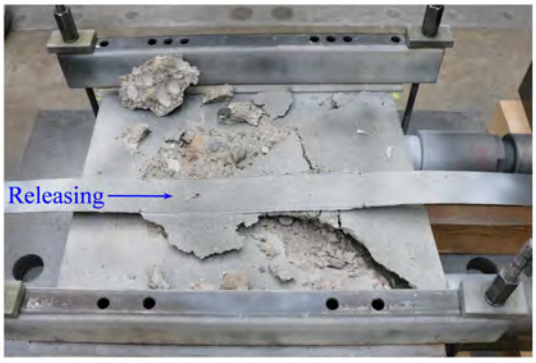

(g) EBROG-10×10-1

(h) EBROG-10×10-2

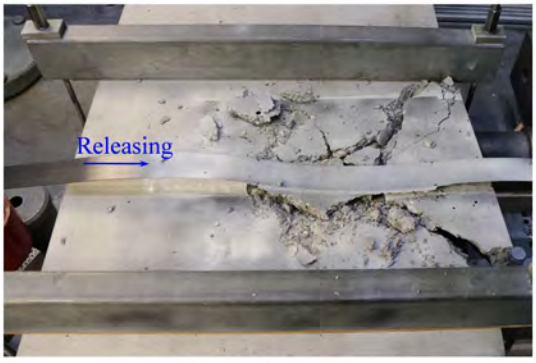

(i) EBROG-10×20-1

(j) EBROG-10×20-2

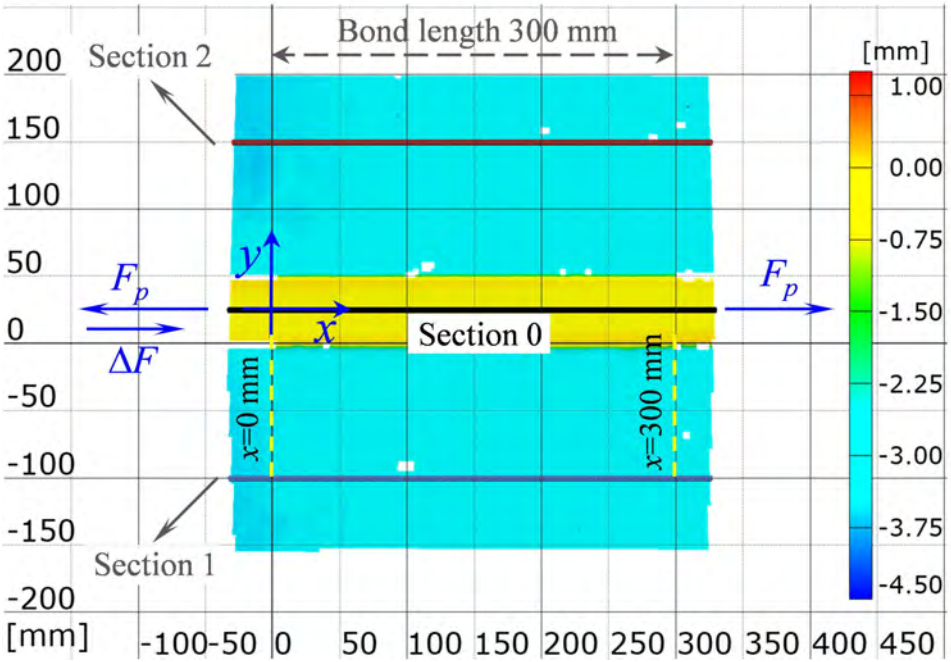

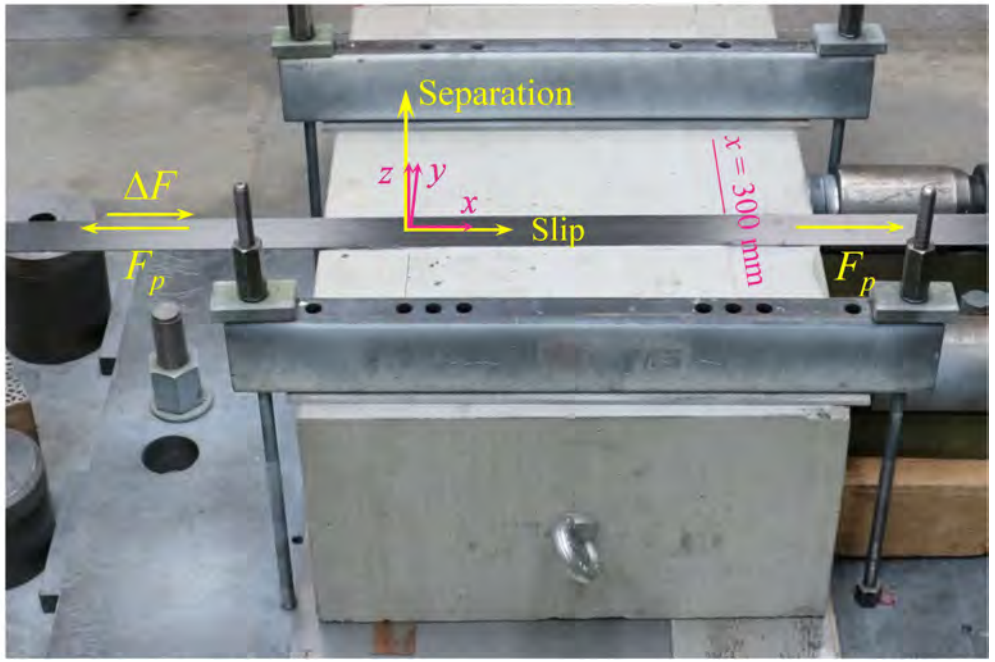

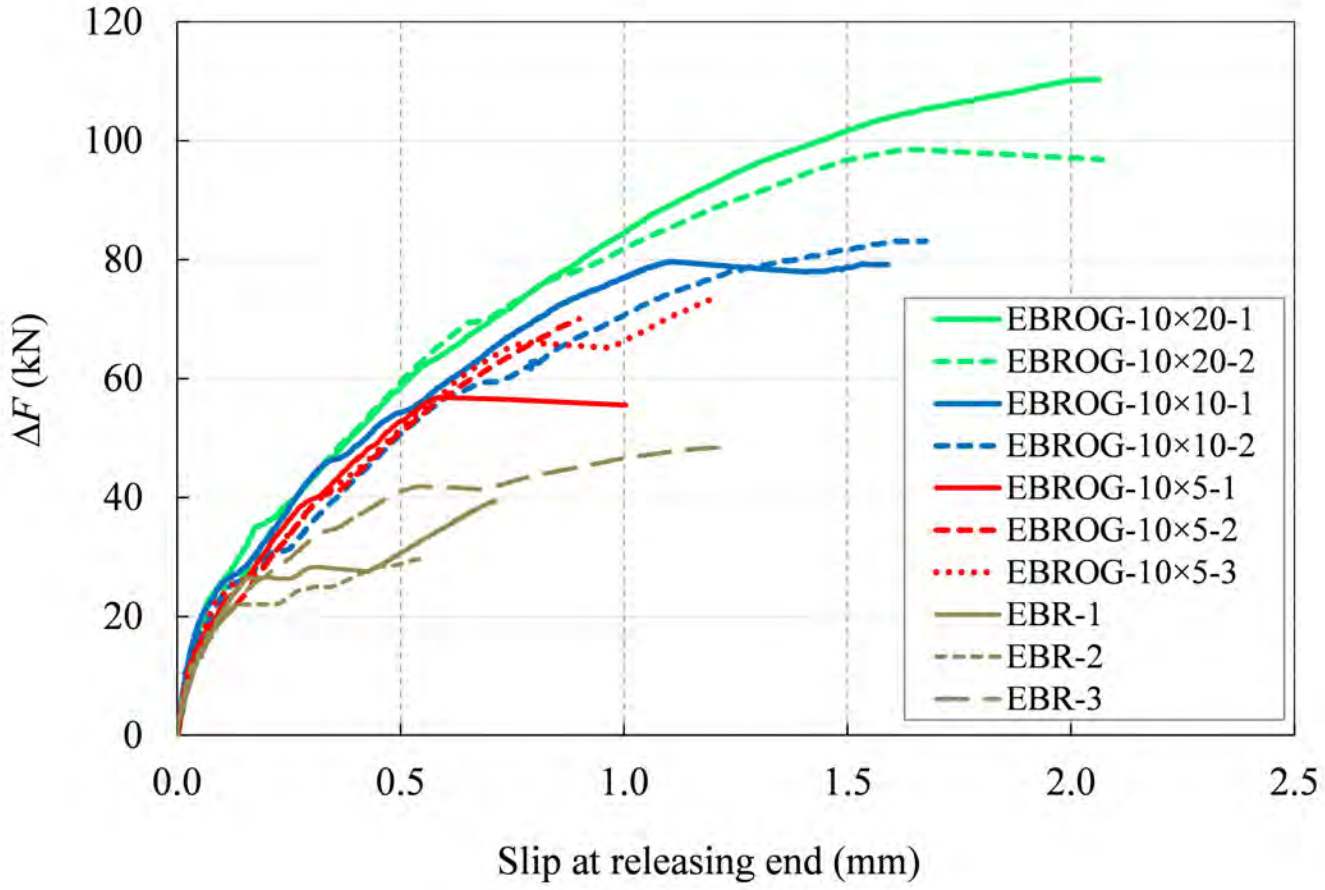

(a) Force-slip

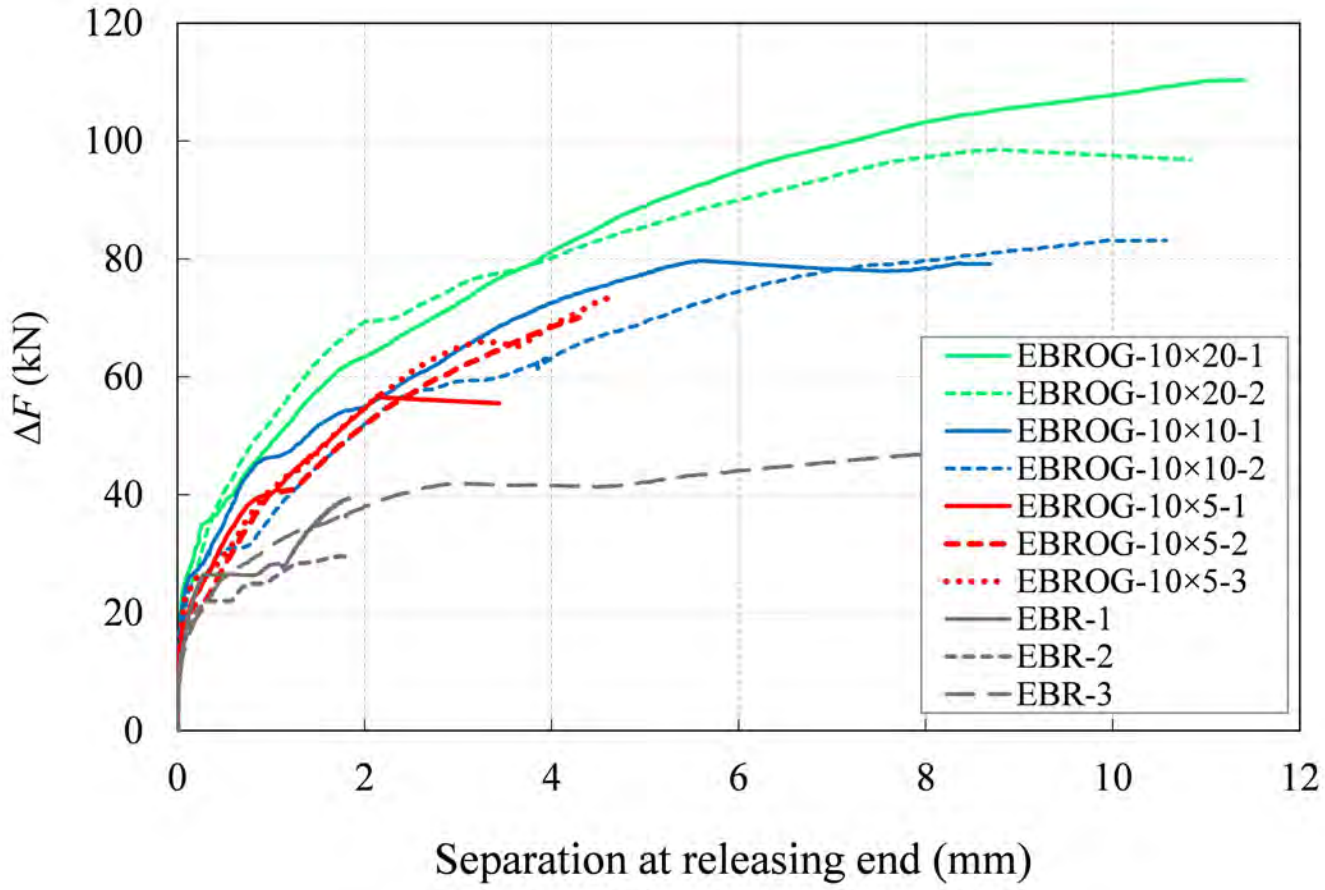

(b) Force-separation

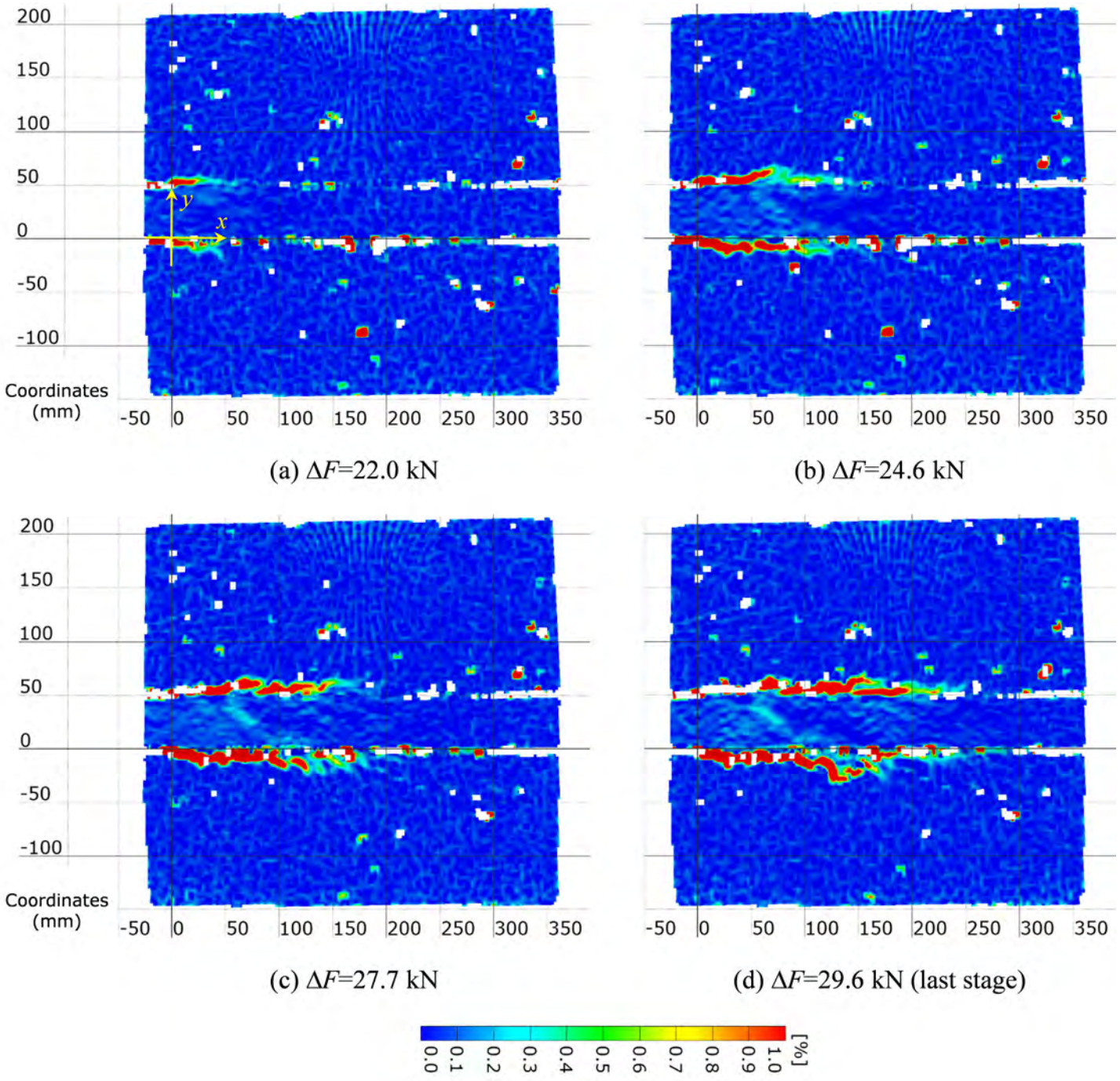

(a) ΔF=22.0 kN

(b) ΔF=24.6 kN

(c) ΔF=27.7 kN

(d) ΔF=29.6 kN (last stage)

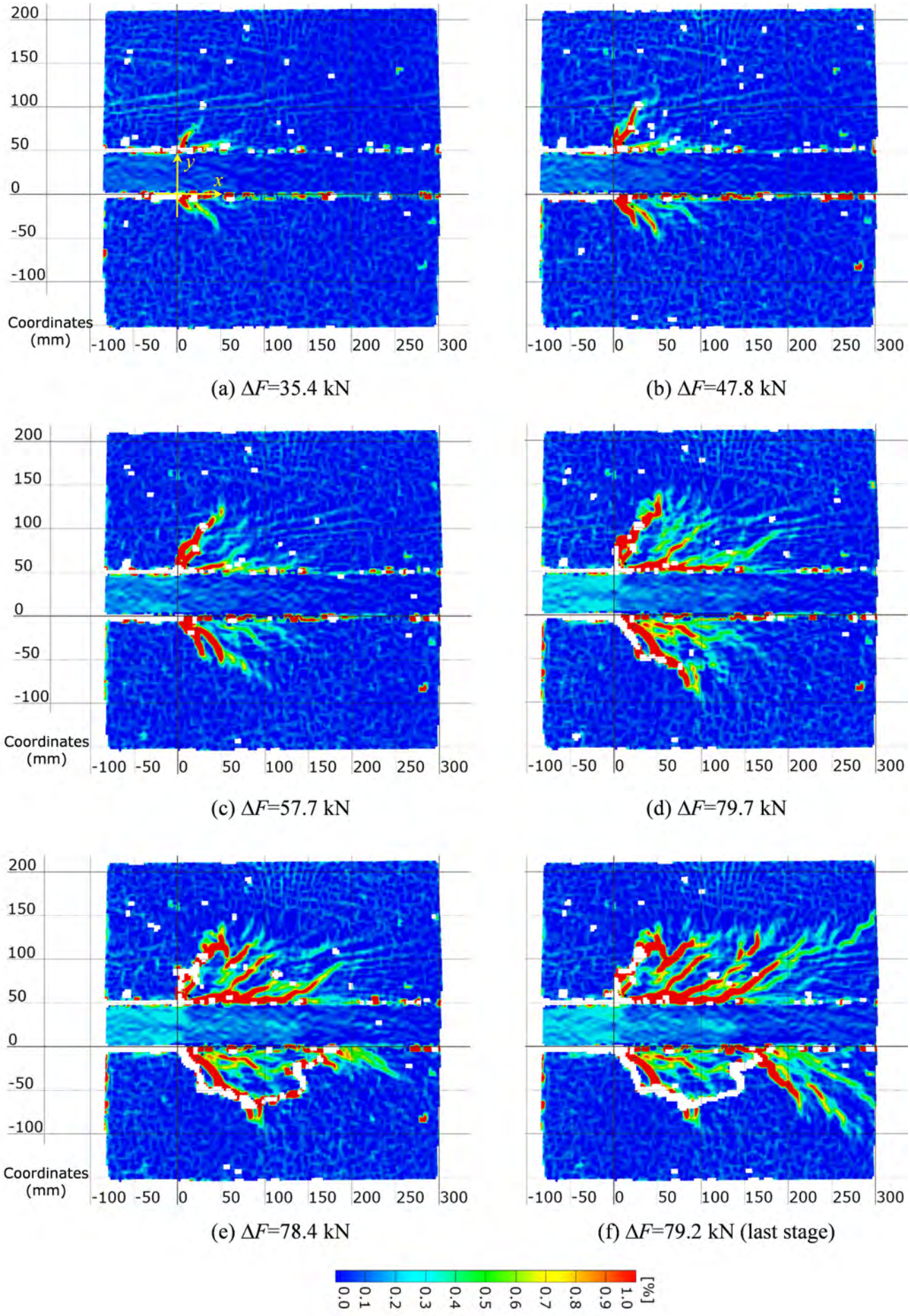

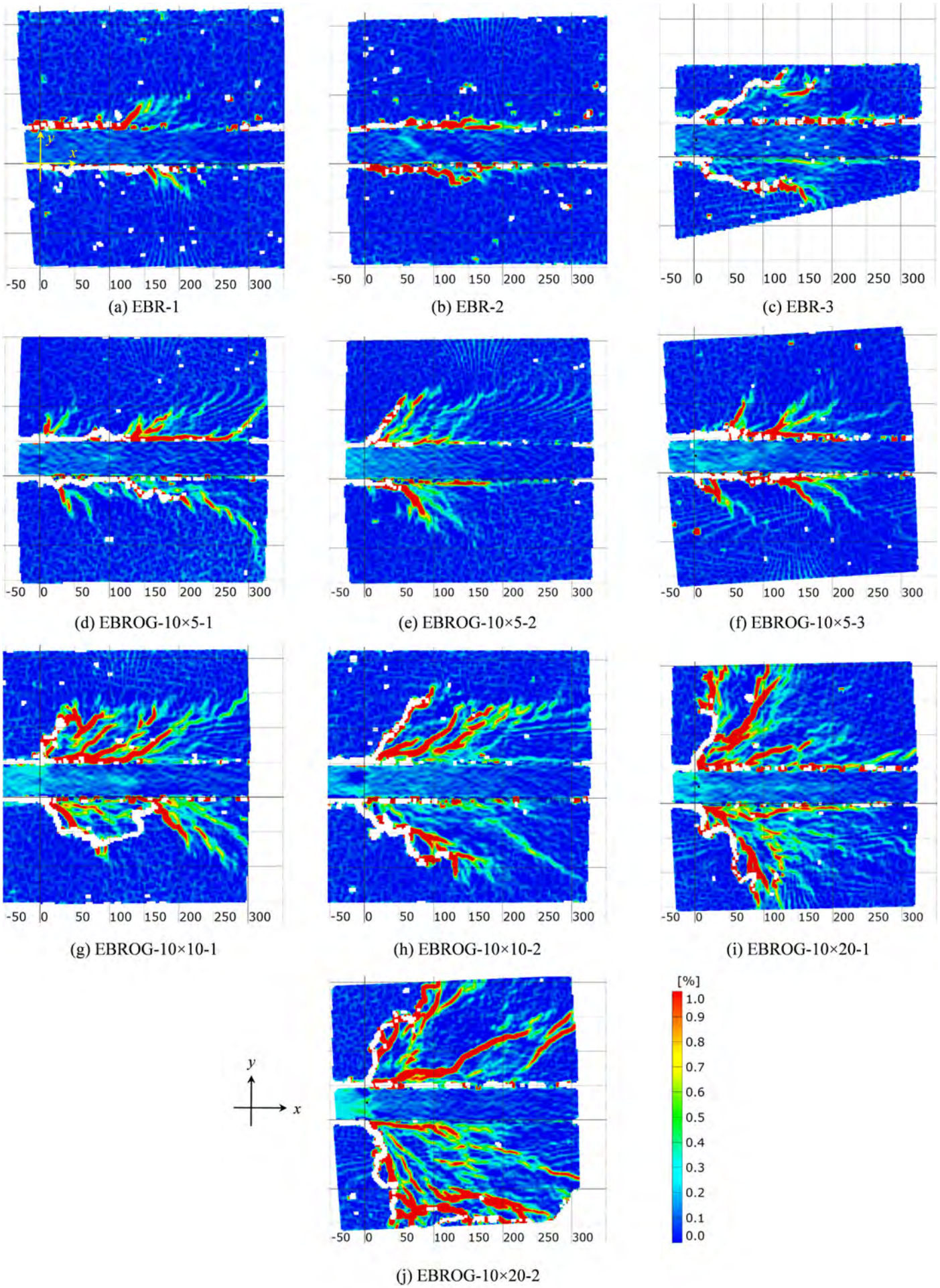

(a) EBR-1 (b) EBR-2 (c) EBR-3

(d) EBROG-10×5-1 (e) EBROG-10×5-2 (f) EBROG-10×5-3

(g) EBROG-10×10-1 (h) EBROG-10×10-2 (i) EBROG-10×20-1

(j) EBROG-10×20-2

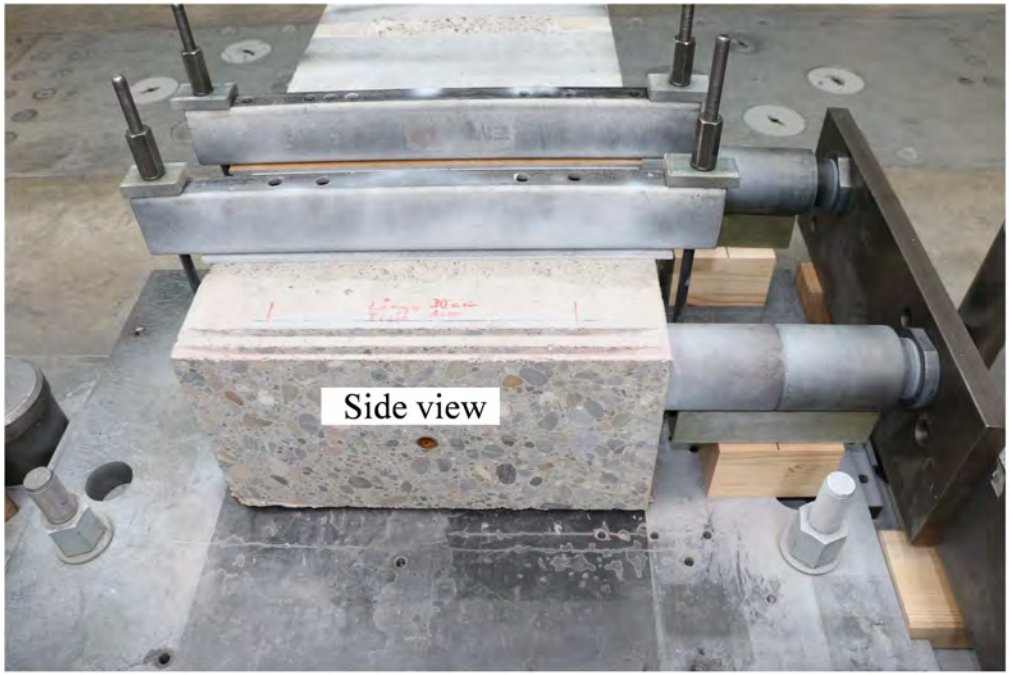

(a) Grooves cut near the block edge

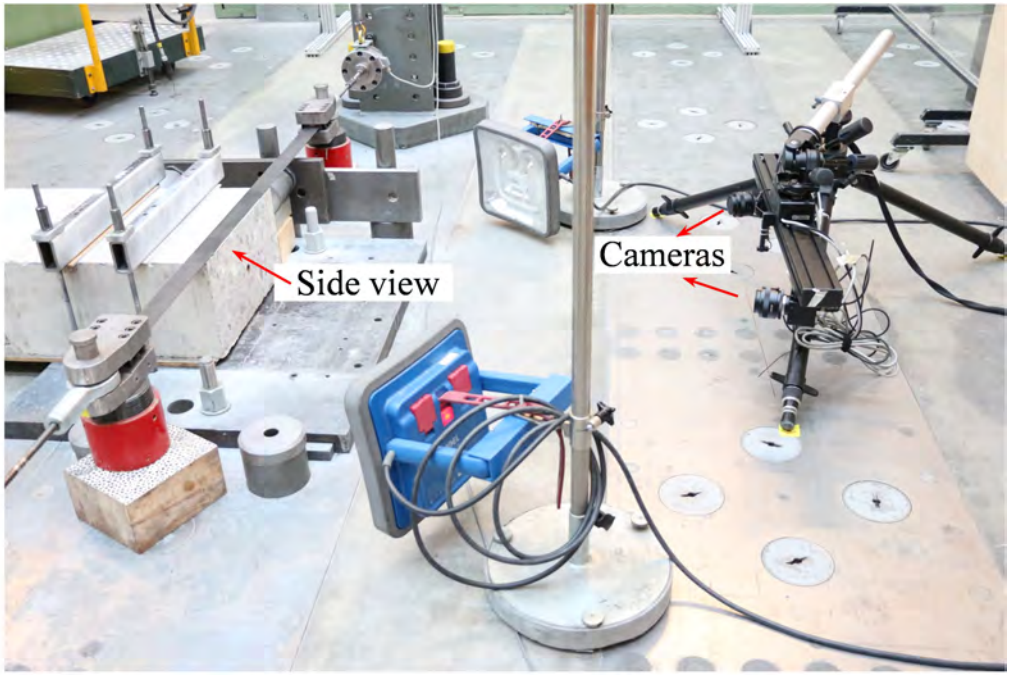

(b) Position of DIC cameras

(a) Side view

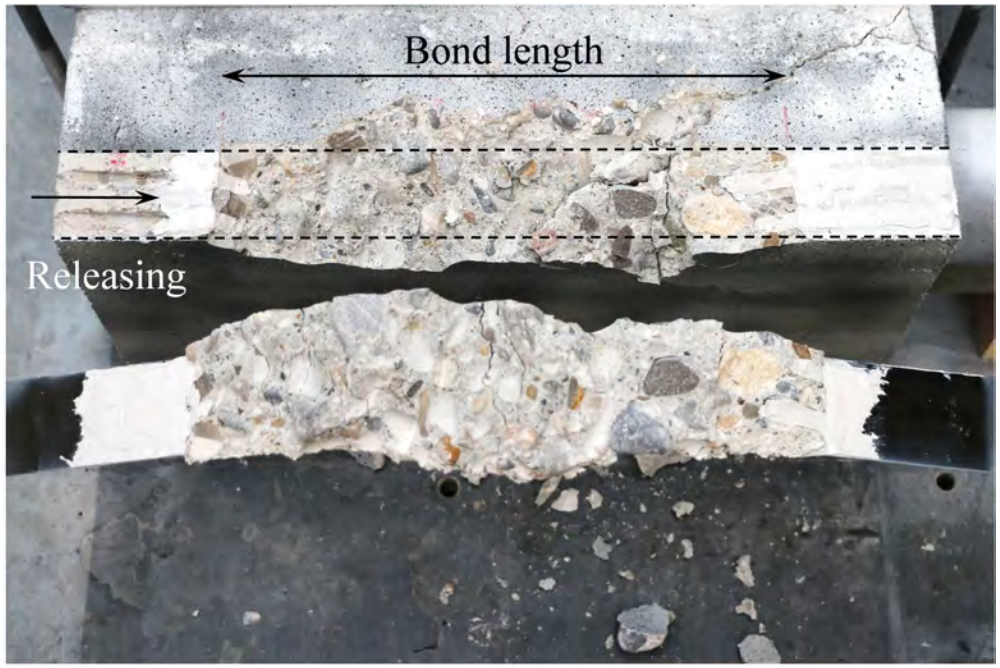

(b) Top view

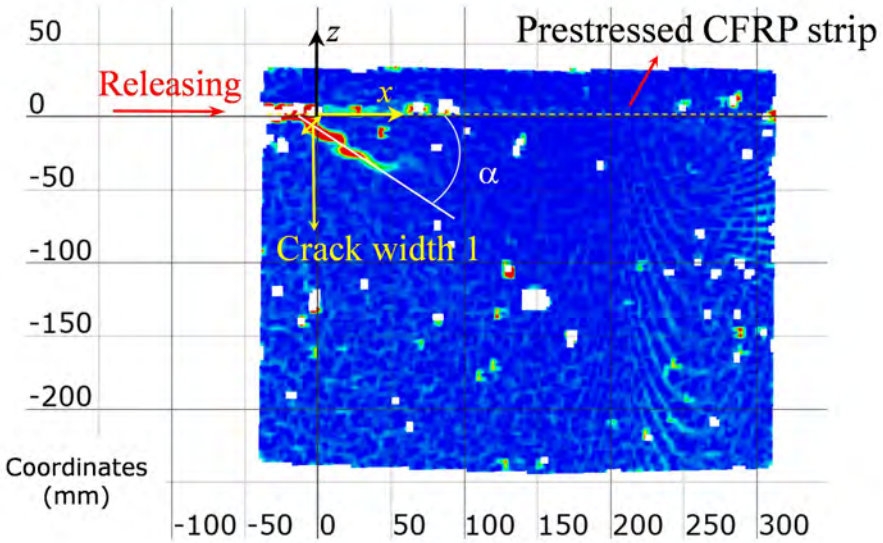

(a) ΔF=24.1 kN

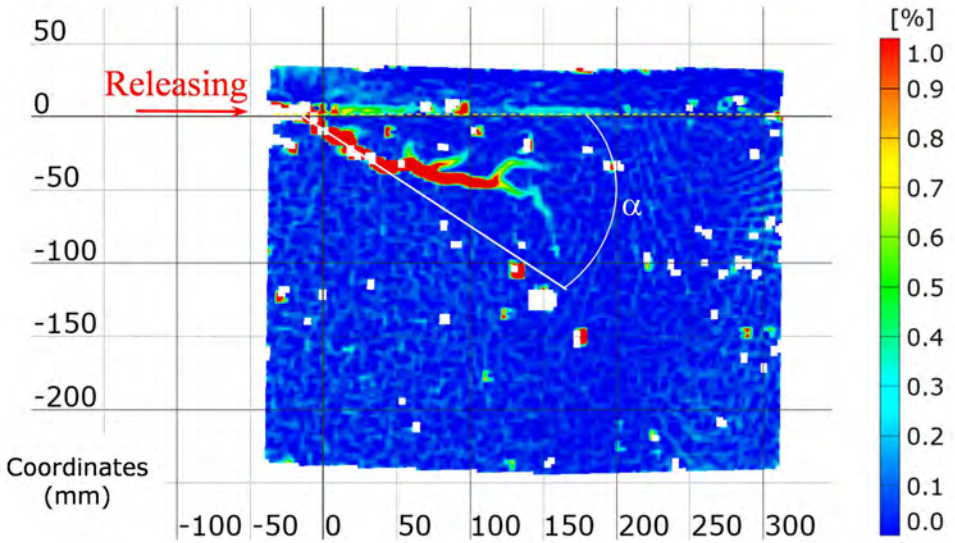

(b) ΔF=34.1 kN

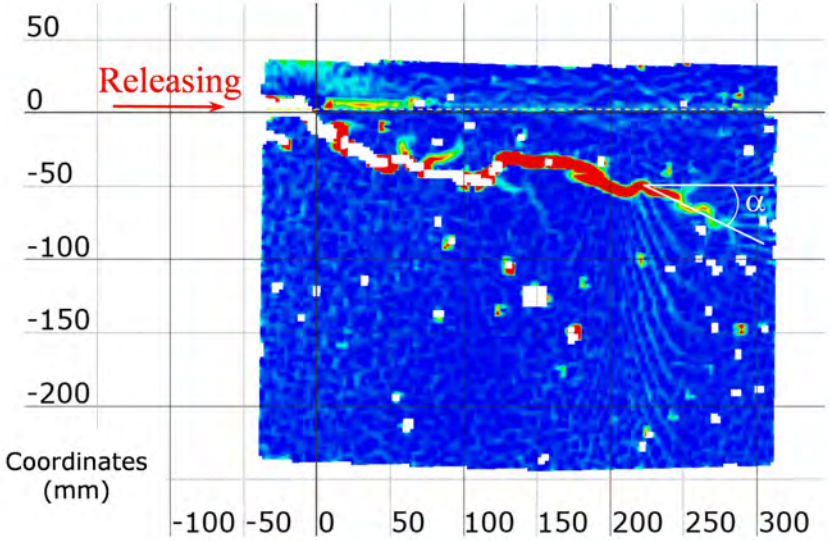

(c) ΔF=39.7 kN (last stage)

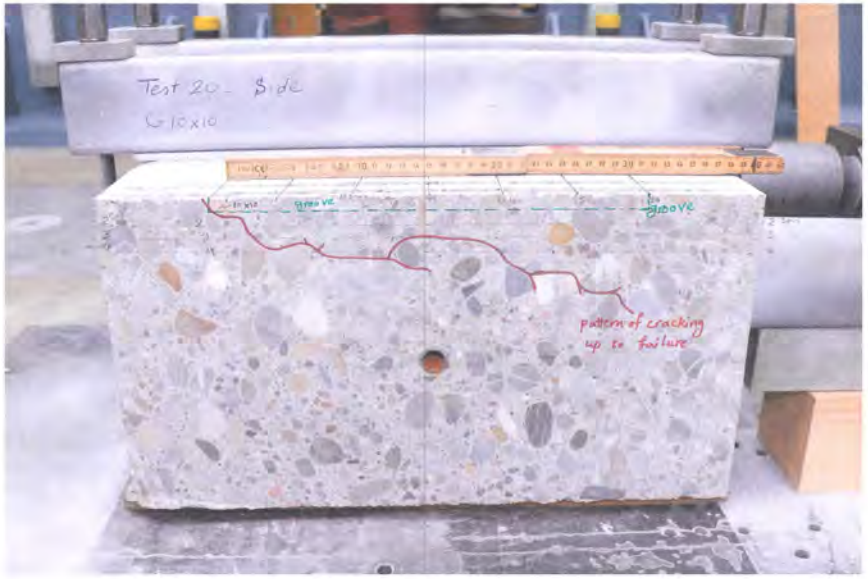

(d) Cracks pattern with respect to the aggregate position, drawn on a photo from the concrete surface

Figure15

Click here to access/download;Figure;Fig. 15 .pdf

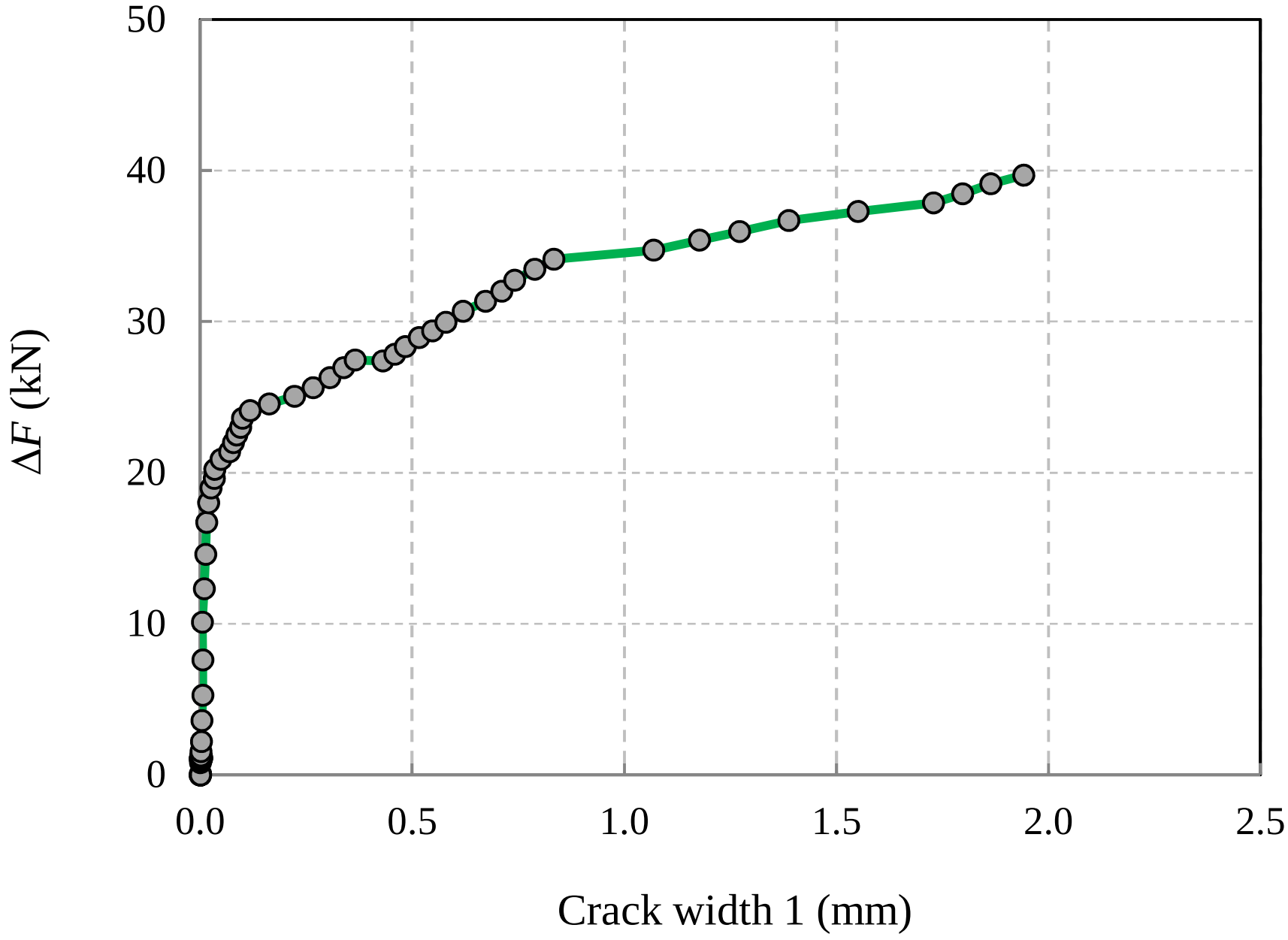

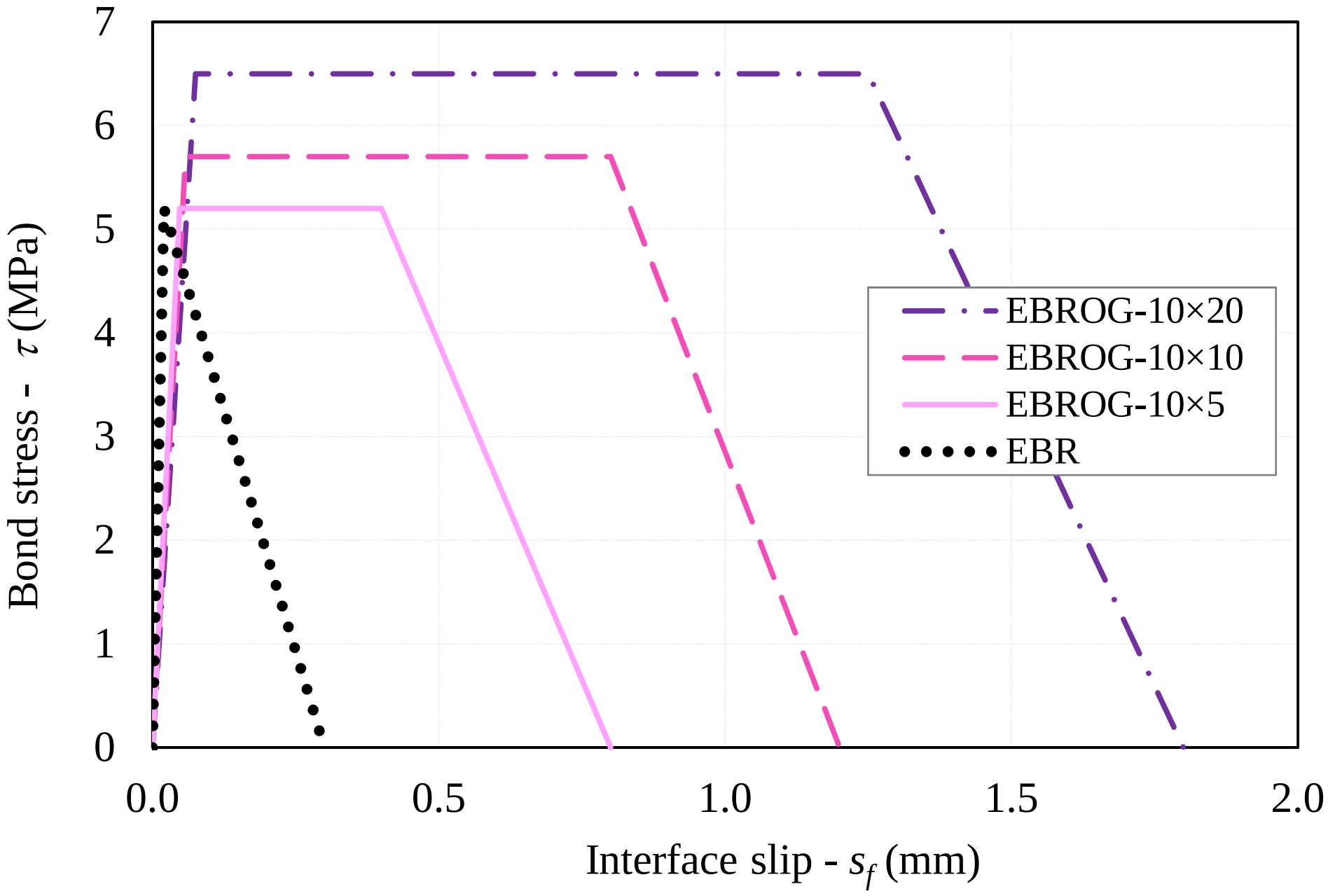

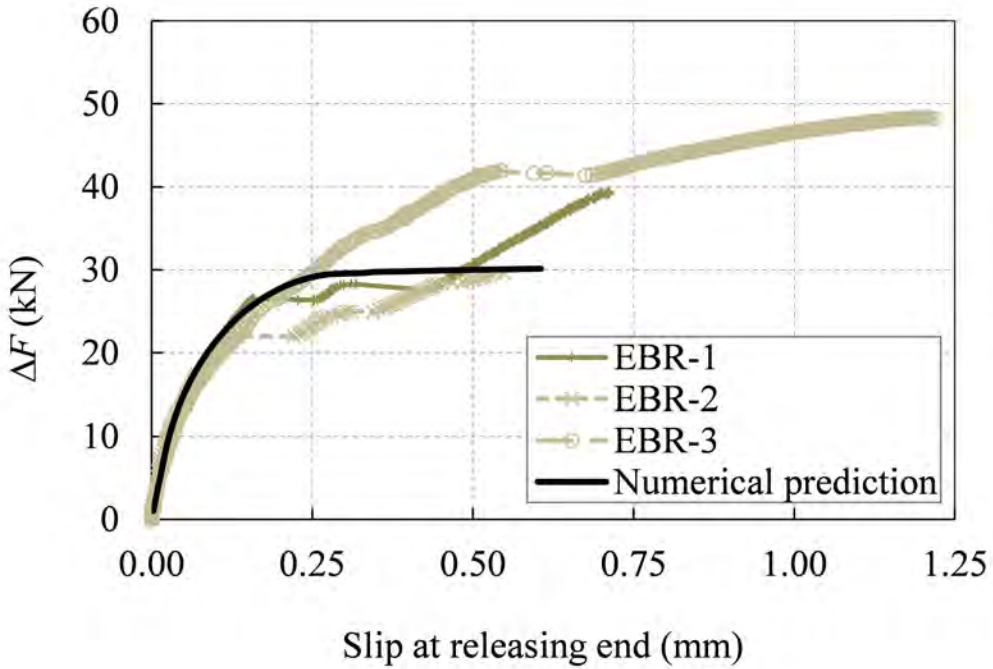

(a) Force-slip relationship

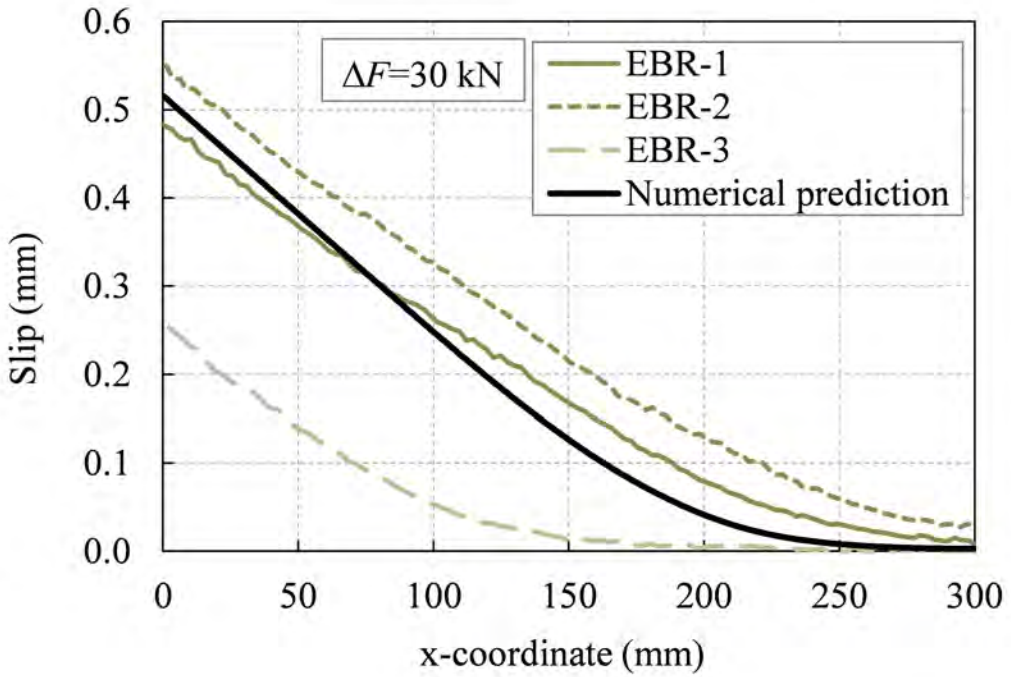

(b) Interface slip distribution (ΔF= 30 kN)

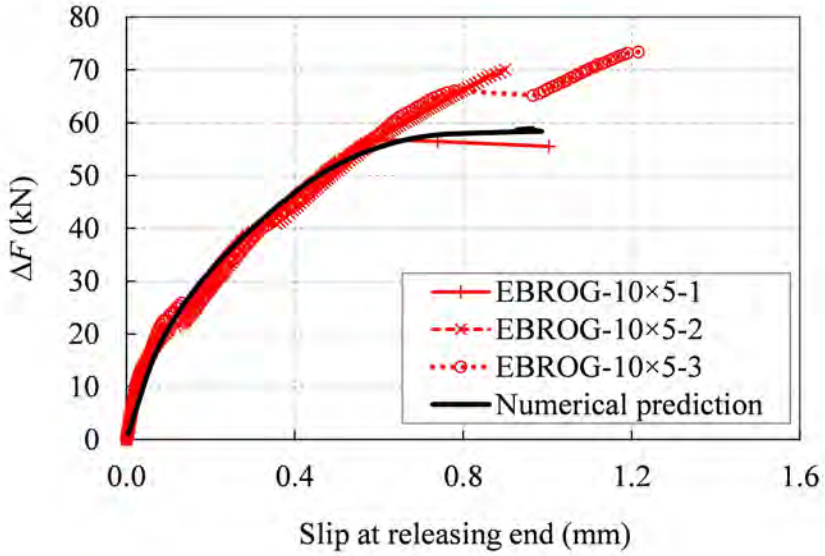

(a) Force-slip relationship

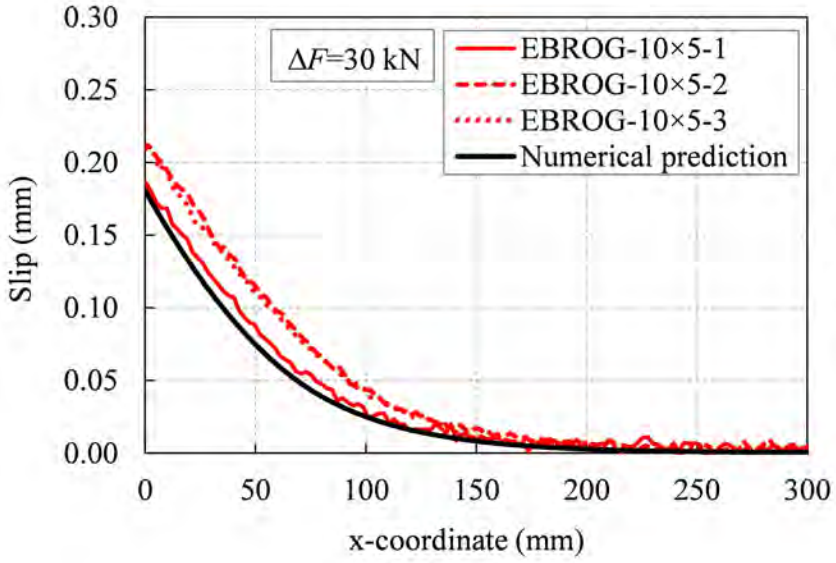

(b) Interface slip distribution (ΔF= 30 kN)

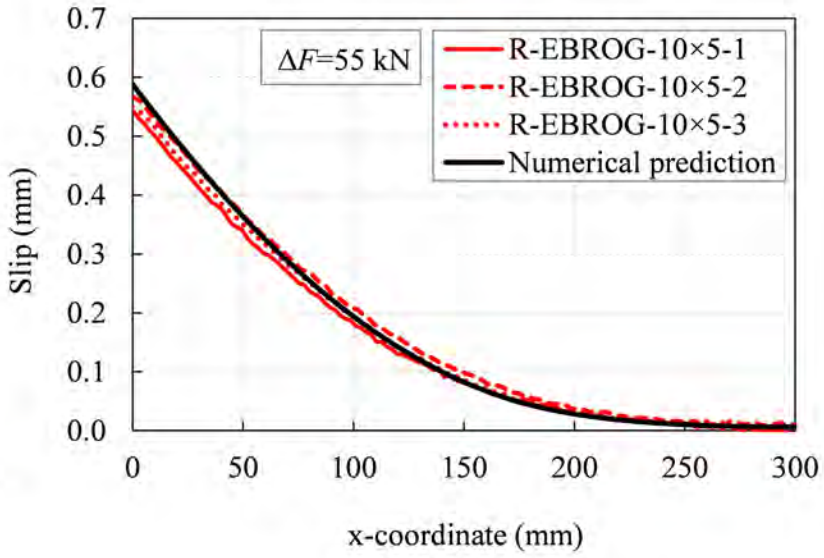

(c) Interface slip distribution (ΔF= 55 kN)

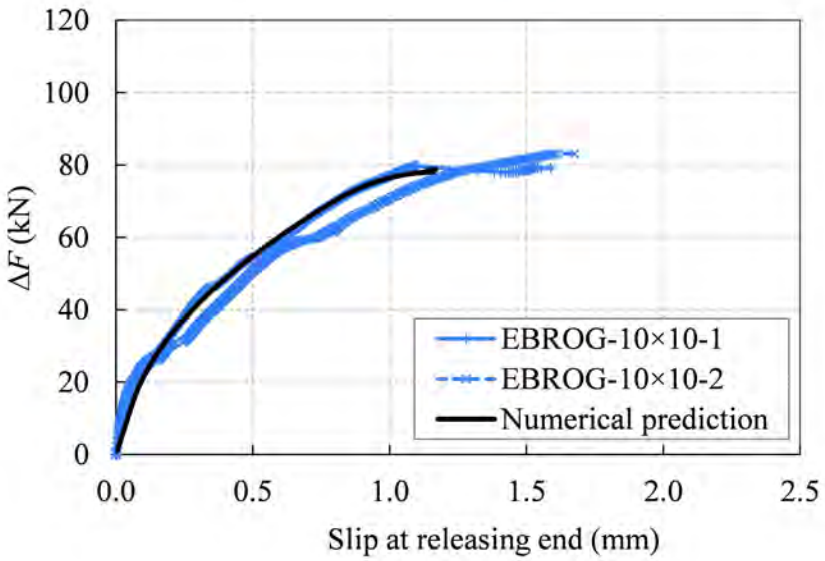

(a) Force-slip relationship

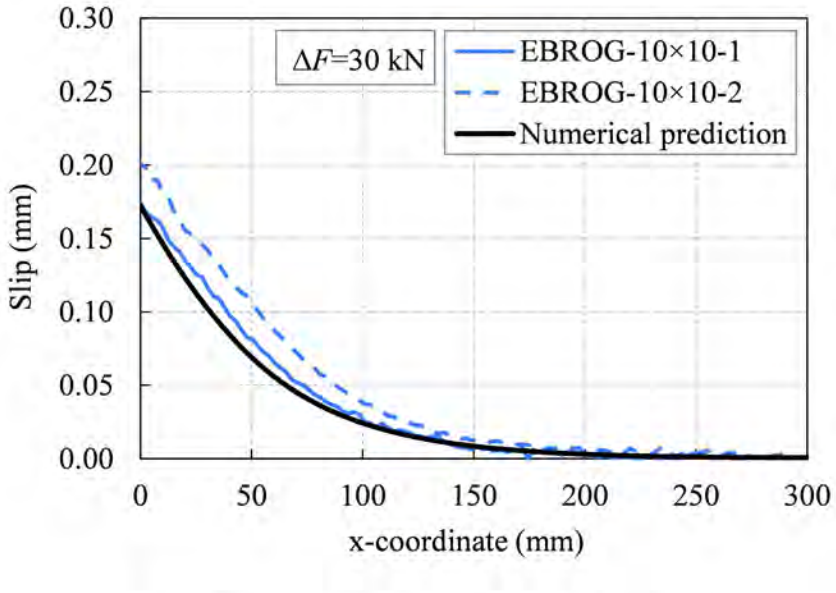

(b) Interface slip distribution (ΔF= 30 kN)

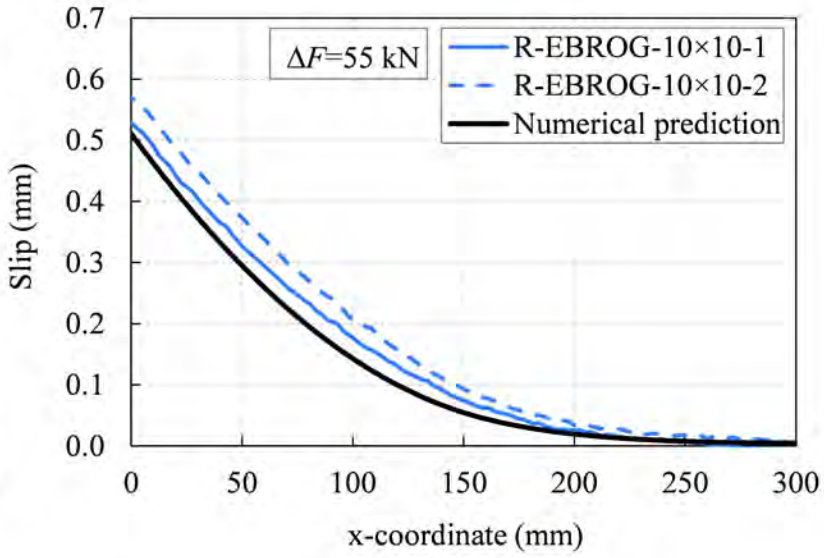

(c) Interface slip distribution (ΔF= 55 kN)

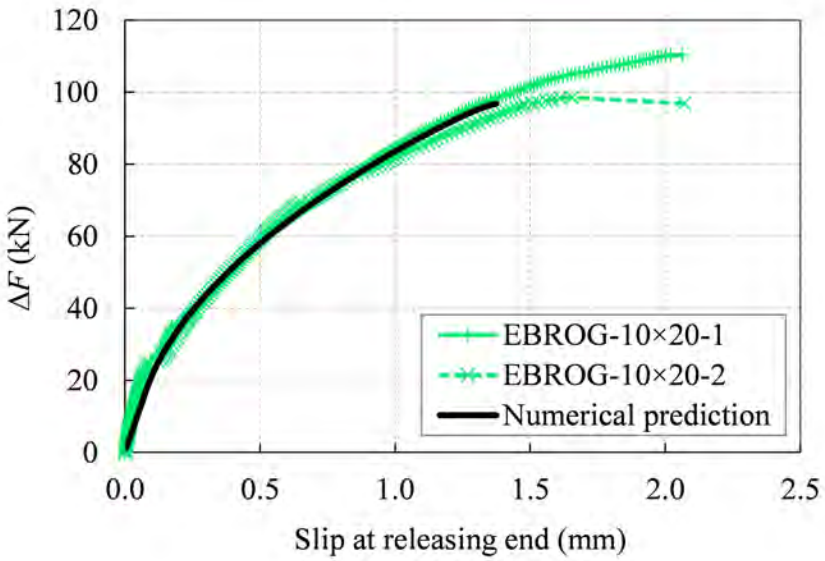

(a) Force-slip relationship

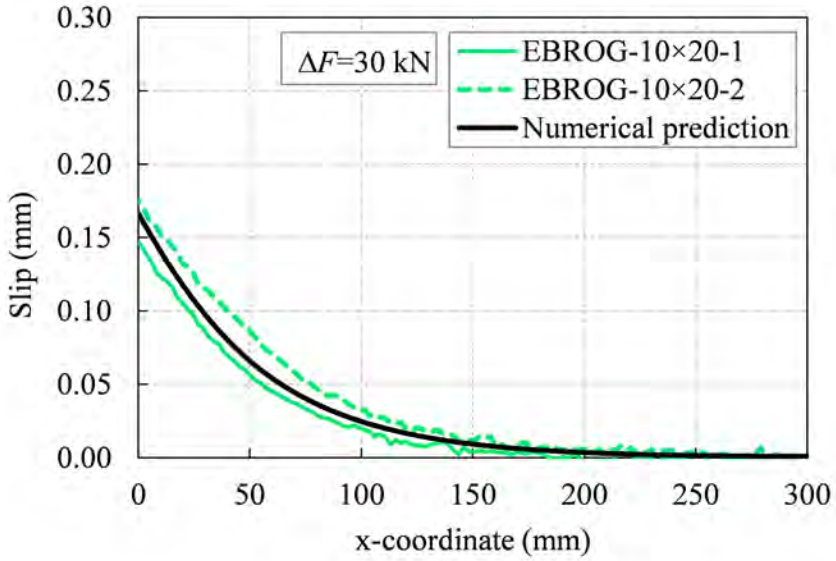

(b) Interface slip distribution (ΔF= 30 kN)

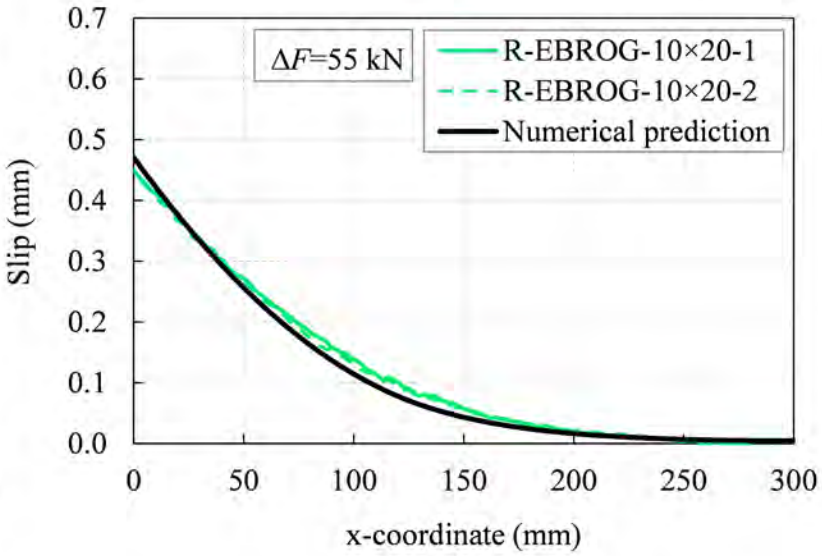

(c) Interface slip distribution (ΔF= 55 kN)